POTENTIAL APPLICATION OF ALTERNATIVE OXIDASE (AOX) IN NEURODEGENERATIVE DISEASES

Yuan Zhuang

Master's degree program in biotechnology (MBIOT)

Department of Biosciences

University of Helsinki

Abbreviation

AD	Alzheimer’s disease
ADP	adenosine diphosphate
ALS	amyotrophic lateral sclerosis
AmpR	ampicillin resistance
AOX	alternative oxidase
ATP	adenosine triphosphate
bp	base pair
BSA	bovine serum albumin
CLB	cell lysis buffer
CMT	Charcot-Marie-Tooth disease
CPEO	chronic progressive external ophthalmoplegia
DAPI	4',6-diamidino-2-phenylindole
DDM	N-Dodecyl-2-D-Maltoside
DMEM	Dulbecco’s modified Eagle's medium
DMSO	dimethyl sulfoxide
EDTA	ethylenediaminetetraacetic acid
EGFP	enhanced green fluorescent protein
EGTA	ethylene glycol-bis(β-aminoethyl ether)-N,N,N',N'-tetraacetic acid
FADH2	flavin adenine dinucleotide
FBS	fetal bovine serum
GAPDH	glyceraldehyde-3-phosphate dehydrogenase
HD	Huntington's disease
HEK293T	human embryonic kidney cells 293T
HEPES	4-(2-hydroxyethyl)-1-piperazineethanesulfonic acid
iPSC	induced pluripotent stem cells
IRES	internal ribosome entry site
LB	lysogeny broth
LHON	Leber’s hereditary optic neuropathy
Midiprep	midipreparation
Miniprep	minipreparation
mtDNA	mitochondrial DNA
NADH	nicotinamide adenine dinucleotide
Ndi1	NADH dehydrogenase
nPG	n-propyl gallate
OXPHOS	oxidative phosphorylation
PBS	phosphate-buffer saline
PCR	polymerase chain reaction
PD	Parkinson's disease
PDL	poly-D-lysine hydrobromide
PES	polyethersulfone
PFA	paraformaldehyde

PLL	poly-L-Lysine
PMSF	phenylmethanesulfonyl fluoride
PVDF	polyvinylidene difluoride
Q	ubiquinone/ubiquinol
RIPA	radioimmunoprecipitation assay buffer
ROS	reactive oxygen species
RT	room temperature
SCAs	Spinocerebellar ataxias
SDHA	succinate dehydrogenase complex flavoprotein subunit A
SDS-PAGE	sodium dodecyl sulfate polyacrylamide gel electrophoresis
SHAM	salicyclhydroxamic acid
TBS	Tris-buffered saline
TLB	tissue lysis buffer
TMPD	N,N,N’,N’-tetramethyl-p-phenylenediamine
TR	rhodamine
U2OS	human bone osteosarcoma epithelial cell
WB	western blotting
WRE	woodchuck hepatitis virus Post-transcriptional Regulatory Element
WT	wild type

Table of Content

1. Introduction: 1

1.1. The structure and function of mitochondria 2

1.1.1 Structure 2

1.1.2 Function 3

1.1.2.1 Oxidative phosphorylation 3

1.1.2.2 Glucose metabolism 4

1.1.2.3 Other functions 5

1.2. Mitochondrial dysfunction and respiratory chain disorders 6

1.2.1. Primary mitochondrial disease 6

1.2.2. Secondary mitochondrial disease 7

1.3. *AFG3L2* gene knock down cell may serve as an in vitro disease model 8

1.3.1. *AFG3L2* gene 8

1.3.2. Mitochondrial dynamics and quality control 9

1.3.3. Loss of *AFG3L2* gene causes OPA1 protein cleavage and mitochondrial fragmentation 10

1.4. Alternative pathway for compensating respiratory chain defects 11

1.4.1. Function and application of alternative oxidase 11

1.4.2. Regulation of AOX activity 13

1.5. Viral vector as a tool to express AOX gene in mammalian cells 14

1.6. Aim of study 16

2. Material and method 17

2.1. Materials 17

2.1.1. Mouse model 17

2.1.2. Chemicals and solution 18

2.1.2.1 Western blotting buffers 18

2.1.2.2 Protein extraction buffers 20

2.1.2.3 Cell culture solutions 20

2.1.2.4 Transfection solutions 22

2.1.2.5 Oxygraph solutions and immunostaining buffers 22

2.2. Methods and techniques 23

2.2.1. Genotyping and gel electrophoresis 23

2.2.2. Protein extraction 24

2.2.2.1. Protein extraction from the cell 24

2.2.2.2. Protein extraction from the tissue 24

2.2.2.3. Measurement of protein concentration 24

2.2.3. Western blotting 25

2.2.3.1. Customized gel protocol 25

2.2.3.2. Commercialized gel protocol 25

2.2.3.3. Stripping 25

2.2.4. Cell culture 26

2.2.4.1. Cell line maintenance 26
2.2.4.2. Antimycin A treatment 27
2.2.4.3. Plate coating 27
2.2.5. Mitochondrial respiration 27
2.2.5.1. Mitochondrial extraction 27
2.2.5.2. Mitochondrial respirometry 28
2.2.6. Construction of AOX lentiviral vector 29
2.2.6.1. Plasmid construction 29
2.2.6.2. Transformation 30
2.2.6.3. Amplification and purification of plasmid DNA 30
2.2.6.4. Viral vector production 31
2.2.6.5. Viral vector infection 32
2.2.7. Immunostaining 32
2.2.7.1. Antibody immunostaining 32
2.2.7.2. Nucleic acid staining 33
2.2.7.3. Imaging 33
2.2.8. Construction of in vitro disease model and AOX rescue test 33
2.2.8.1. AOX infection on U2OS cell model 33
2.2.8.2. AFG3L2 siRNA double transfection 34
2.2.8.3. Identification of protein expression and mitochondrial fragmentation 34
2.2.9. Statistical analysis 35
3. Results 35
3.1. Low expression of AOX in the brain of 1-month-old hemizygous *AOX*^{Rosa26} transgenic mouse 35
3.2. AOX expression in the primary neuro-glia cells of new born mice 36
3.3. Antimycin A resistance of primary neuro-glia cells expressing AOX 37
3.4. Buffer optimization for tissue protein extraction 39
3.5. AOX expression in the brain of different ages of hemizygous *AOX*^{Rosa26} transgenic mice 40
3.6. Mitochondrial respiratory activity in the brain and liver of hemizygous *AOX*^{Rosa26} transgenic mice 41
3.7. AOX viral vector construction and infection on U2OS cells 43
3.8. *AFG3L2* gene knock down in vitro model and AOX lentivirus rescue 45
4. Discussion 49
4.1. AOX expression and activity in the transgenic mouse brain 49
4.2. Lentiviral vector construction and AOX expression in virus infected cells 53
4.3. AOX function and application in the neurodegenerative disease model in vitro 55
5. Conclusion 60
6. Acknowledgements 61
7. References 62

1. Introduction:

In most eukaryotic organisms, there is a double-membrane-bound organelle called mitochondrion, which acts as a powerhouse of the cell (Henze and Martin, 2003). The mitochondrion is responsible for the aerobic respiration in eukaryotic cells, converting carbohydrates and oxygen into adenosine triphosphate (ATP) by the process of oxidative phosphorylation (Cooper, 2000). According to a popular hypothesis about the origin of mitochondrion, the mitochondrion arose from an aerobic prokaryote, which was then engulfed by an anaerobic nucleated cell as endosymbiosis (Marten and Mentel, 2010). Therefore, the nucleated cell acquired a more efficient way of producing energy with the help of mitochondria and evolved to modern eukaryotes. This origin may explain why mitochondria have their own genome. Although most genes encoding mitochondrial proteins have been transferred into the nucleus during evolution, the genes that remain in the mitochondria are essential for the transcription and translation of certain inner-membrane protein subunits (Alberts et al., 2015).

Mitochondria are known to play an important role in aging and many cellular processes, such as energy production, glucose metabolism and cell signaling. If mitochondria are unable to function properly in the cell, they may impact the health of the organism. Some neurodegenerative diseases including Alzheimer's disease (AD), Parkinson's disease (PD), amyotrophic lateral sclerosis (ALS) and Huntington's disease (HD) are considered to involve mitochondrial dysfunction and blockade of mitochondrial respiratory chain (Lin and Beal, 2006). Unfortunately, most of the mitochondrial disorders lack effective treatments.

To seek a potential therapy for mitochondrial diseases, an alternative oxidase (AOX) originated from *Ciona intestinalis*, has been applied to counteract the defects of mitochondrial respiratory chain in mice (El-Khoury., 2013). Additionally, previous studies on plants (Maxwell et al., 1999), drosophila (Liu et al., 2007) and human cultured cells (Dassa et al., 2009) have strongly supported that the expression of AOX provides a bypath of blocked respiratory chain, reducing the reactive oxygen species

(ROS) and ameliorating cell damages. These inspiring results indicate that AOX may be a promising tool for curing mitochondrial diseases. Therefore, an engineered mouse model has been created to express the *Ciona intestinalis AOX* ubiquitously in the whole animal so that the function of AOX can be studied in the mammalian system comprehensively (Szibor et al., 2017).

1.1. The structure and function of mitochondria

1.1.1 Structure

The complex structure of mitochondrion is formed by two specialized membranes, segregating the intact organelle into two compartments: the intermembrane space and the internal matrix. These membranes are critical for defining distinct functions of mitochondria due to different transmembrane proteins located on each membrane.

The outer mitochondrial membrane is similar to the eukaryotic plasma membrane. It encloses the entire organelle and allows free diffusion of all the molecules that weigh 6000 daltons or less through certain membrane proteins called porins, making the composition of small molecules and pH uniform between the intermembrane space and the cytosol (Alberts et al, 2015).

The inner membrane is more selective to the molecules that pass through it. Since the membrane has a large amount of cardiolipin, most of hydrophilic molecules are efficiently isolated outside the membrane, especially the ions (Alberts et al, 2015). This characteristic provides an ideal environment for the enzymes in the matrix to perform specific metabolic reactions, as only essential molecules can be imported into the matrix by certain transport proteins. Besides the specific transport proteins, the inner membrane also harbors a variety of functional enzymes, including the ATP synthase and respiratory enzyme complexes. The inner membrane folds on itself to form massive convoluted structures called cristae, which largely increases the surface area of the inner membrane, enabling more functional protein complexes to settle

down.

The internal compartment enclosed by the inner membrane is the matrix, where the mitochondrial genome and ribosome as well as a variety of metabolic enzymes are located. The matrix is the most important place for the citric acid cycle of oxidative metabolism. Pyruvate and fatty acids, derived from sugars and fats respectively, can be converted to acetyl CoA in the matrix and further oxidized for fuels through the citric acid cycle. Therefore, the matrix contains the majority of enzymes catalyzing the oxidation of fatty acids and carbohydrates.

1.1.2 Function

1.1.2.1 Oxidative phosphorylation

The most prominent contribution of mitochondria is the energy they produces for the cell. The major energy is produced in the form of ATP, through a series of redox reactions during aerobic respiration, or specifically oxidative phosphorylation. There are four complexes involved in this process, namely NADH dehydrogenase, succinate dehydrogenase, cytochrome *c* reductase, and cytochrome *c* oxidase, widely known as complex I, II, III, and IV, respectively (Berg et al., 2002; Alberts et al., 2015). These complexes are embedded in the inner mitochondrial membrane and serve as electron transporters. Altogether, they form a respiratory chain as electron carriers and pump protons across the inner membrane of mitochondria, generating an electrochemical gradient between mitochondrial matrix and crista space. This electrochemical gradient drives both ATP synthesis and active transport of specific molecules across the mitochondrial membrane.

The sophisticated redox reactions in the respiratory chain can be divided into three stages (see Fig 1). In the first stage, complex I transfers two electrons from the reduced form of nicotinamide adenine dinucleotide (NADH) to an electron-carrier called ubiquinone (Q), pumping four protons from the matrix to the intermembrane

space. Ubiquinone also takes electrons from the reduced form of flavin adenine dinucleotide ($FADH_2$) through complex II. However, complex II pumps no proton across the inner mitochondrial membrane. The second stage happens in the complex III, where the electrons carried by the reduced form of Q (ubiquinol) are transferred to cytochrome *c*, and four protons are pumped outside the inner membrane. Therefore, the ubiquinol returns to its original state. The reduced cytochrome *c* generated by complex III is finally oxidized by complex IV in the last stage, along with the reduction of oxygen to two molecules of water. Thus, four more protons are transferred through the inner membrane (Berg et al., 2002).

After the three stages of redox reactions, the ATP synthase, also called complex V, carries out phosphorylation reactions to produce energy. Based on the chemiosmotic coupling hypothesis (Mitchell P, 1966), the proton gradient generated by the electron transport chain promotes the translocation of protons of higher concentration in the intermembrane space, back to the matrix through the ATP synthase. This flux releases a large amount of free energy that is then used by the ATP synthase to drive phosphorylation of adenosine diphosphate (ADP), storing the free energy in a chemical form so that it can be utilized in other biochemical reactions.

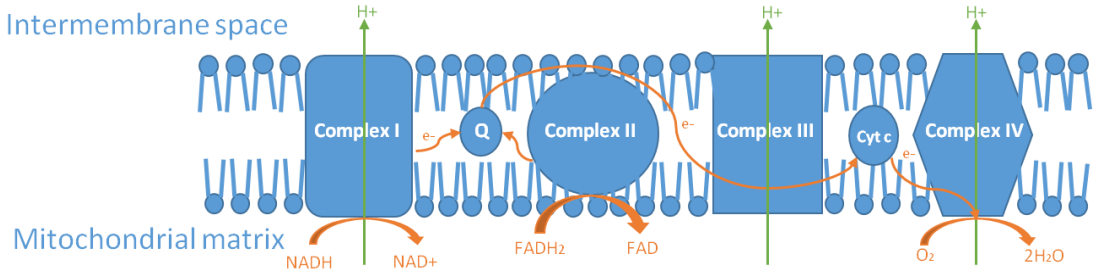

Fig 1. The electron transportation pathway in the mitochondrial respiratory chain

The main components consisting of the mitochondrial respiratory chain are shown. In the respiratory chain, electrons (*orange thin arrows*) are transferred from NADH and $FADH_2$, passed by Complex I, Complex II, Complex III as well as electron carriers ubiquinone (Q) and cytochrome *c* (Cyt c), finally accepted by the O_2 to produce H_2O through Complex IV. Complex I, III and IV pump out protons (*green arrows*) from mitochondrial matrix to intermembrane space during this process.

1.1.2.2 Glucose metabolism

Mitochondrion is not only a powerhouse for the cell, it also plays an important role in glucose metabolism. Although glycolysis, the first step of glucose metabolism, starts in the cytoplasm, the metabolic products of glycolysis are highly involved in biochemical reactions of mitochondria. As mentioned in the end of 1.1.1, pyruvate is decarboxylated in the mitochondrial matrix to produce acetyl CoA, which is the common metabolite of catabolisms of carbohydrate, lipid and protein. Acetyl CoA is also the primary substrate of the citric acid cycle (Krebs and Johnson, 1937). As the final pathway of these essential catabolisms, the citric acid cycle is responsible for oxidizing nutrients absorbed by organisms into carbon dioxide and water. During this process, the citric acid cycle generates many intermediate metabolites, which also participate in other metabolisms such as lipid and amino acid synthesis. Moreover, the citric acid cycle saves a great amount of energy in the form of NADH, coupled with the electron transport chain and ATP synthesis (Voet et al, 2013).

1.1.2.3 Other functions

In addition to the indispensable contribution in the energy production and glucose metabolism, mitochondria are involved in a number of critical cellular metabolisms. For example: the calcium homeostasis, is controlled by both the endoplasmic reticulum and the mitochondrial calcium uniporter (Kirichok et al, 2004). The thermogenic function in brown adipose tissue is also related to an uncoupling protein UCP1 embedded in mammalian mitochondrial inner membrane (Mozo et al, 2005). Furthermore, mitochondria even affect various key events of cell cycle and apoptosis (Green and Reed, 1998).

Interestingly, the morphology of mitochondria is not invariable. Studies about mitochondrial dynamics have implied that the morphology of mitochondria plays a role in cell signaling, tissue development and neuronal functions (McBride et al, 2006).

According to the important functions mentioned above, it is significant to learn about

mitochondria. This small organelle contains big potential to maintain human health, cure diseases, and delay senescence.

1.2. Mitochondrial dysfunction and respiratory chain disorders

Given all the benefits provided, the mitochondrion holds a fundamental position in the human body. On the other hand, defects of mitochondrial function may lead to severe health problems. As a result of dysfunction of mitochondrial respiratory chain, a variety of symptoms can arise in different tissues, including muscle weakness, heart failure, dementia, optic or auditory disorders, developmental delay and respiratory complications (Federico et al., 2012). Based on the cause of mitochondrial dysfunction, most of mitochondrial diseases can be divided into two categories: either of primary or secondary origin. A primary mitochondrial disease results from mutations in the mitochondrial genome or nuclear gene that encodes mitochondrial proteins; while a secondary mitochondrial disease results from both of the damaged genes and external environmental or pharmacologic factors (Filler et al., 2014). Commonly, mitochondrial dysfunction has been treated as a rare disease. However, due to a lack of accurate diagnostic methods for this dysfunction, the prevalence of mitochondrial diseases is likely to be underestimated. By 2008, the estimated rate of having mitochondrial diseases was about 9.2 in 100,000 people, and a further 16.5 in 100,000 people were at risk for developing this sort of disease (Schaefer et al., 2008).

1.2.1. Primary mitochondrial disease

The mitochondrion has its own DNA (mtDNA), which encodes the mitochondrial proteins involved in the respiratory chain. Defects or mutations of mtDNA may cause numerous mitochondrial disorders, especially in the oxidative phosphorylation (OXPHOS) system. Myopathies such as chronic progressive external ophthalmoplegia (CPEO) are the most commonly manifested symptom for mtDNA

defects of OXPHOS in clinical (Leonard and Schapira, 2000). Similarly, encephalomyopathies and Leber's hereditary optic neuropathy (LHON) are also associated with defective mitochondrial genes. Even if mtDNA defects can affect every tissue in the body, muscle and brain are often more severely affected than other tissues because of their high dependence on the energy provided by OXPHOS. More complications can be developed in multiple systems later on. Due to the maternal inheritance of mitochondria, these diseases always show a maternal inheritance in the offspring.

Except for the small amount of mitochondrial genes, most of gene products that compose the proteins of mitochondrial respiratory chain are still expressed and transported from the nuclear DNA (DiMauro and Schon, 2003). Mutations in these genes will lead to mitochondrial diseases as well. For example, mutated genes of nuclear-encoded Complex II subunits can result in Leigh's syndrome, which is a neurologic disorder arising from childhood. Moreover, a NADH-binding-site encoded gene mutation in the nuclear genome can even cause myoclonic epilepsy psychomotor delay and leukodystrophy in children. (Leonard and Schapira, 2000)

1.2.2. Secondary mitochondrial disease

Not all mitochondrial diseases are caused by the genes that maintain the structure and function of mitochondrial respiratory chain. Proteins that are responsible for the transportation or assembly of mitochondrial proteins may also result in disorders within OXPHOS system. Deficiencies of non-OXPHOS mitochondrial proteins that lead to respiratory chain dysfunction, belong to a second type of mitochondrial disease. Compared with primary mitochondrial diseases, the secondary mitochondrial diseases are more complicated in clinical manifestations. Many neurodegenerative diseases are involved in this group, including Friedreich's ataxia, Hereditary spastic paraparesis, Epilepsy, Alzheimer's disease, Wilson's disease, Huntington's disease and Parkinson's disease (Leonard and Schapira, 2000). The secondary mitochondrial

diseases are generally inherited by autosomal inheritance or emerge sporadically instead of maternal inheritance.

Owing to the heterogeneity of molecular backgrounds, the underlying mechanisms of mitochondrial dysfunction remain unclear. Therefore, neither curative treatment nor proper diagnostic method for mitochondrial diseases has been established (Khan et al., 2015). Most of the available therapies aim at alleviating the symptoms derived from these diseases (Suomalainen, 2011). However, various mouse models have been widely applied to the mitochondrial research, conferring promises to expand the knowledge about mtDNA maintenance and develop new therapies for mitochondrial diseases (Tyynismaa and Suomalainen, 2009).

1.3. *AFG3L2* gene knock down cell may serve as an in vitro disease model

Spinocerebellar ataxias (SCAs) are autosomal dominantly inherited ataxias that belong to neurodegenerative disorders. Patients with these diseases show significant neuronal cell degeneration in the cerebellum and have weak control of muscles (Paulson,H.L, 2009). The genetic causes of many SCAs have been discovered so far, one example is the spinocerebellar ataxias 28 (SCA28). SCA28 is a slowly progressive ataxia resulting from cerebellar damage at onset from early adulthood. Based on the sequence analysis, mutations in the *AFG3L2* gene were the only known genetic defects that lead to SCA28 (Di Bella et al., 2010; Brussino, 2013).

1.3.1. *AFG3L2* gene

AFG3L2 gene encodes a subunit of the m-AAA metalloprotease in the mitochondrial inner membrane and is closely related to paraplegin (Atorino et al., 2003). The m-AAA metalloprotease is involved in mitochondrial protein quality control process, including turnover of mistranslated mitochondrial protein and respiratory chain

complexes assembly (Juhola et al., 2000). Therefore, mutated *AFG3L2* gene encoding deficient m-AAA metalloprotease can lead to proteolytic defects, dysfunction of mitochondrial respiratory chain and excessive ROS production. Since *AFG3L2* gene is highly expressed in human cerebellar Purkinje cell and crucial for axonal development (Maltecca et al., 2008), haploinsufficiency of this gene can cause neurodegeneration in the cerebellum (Maltecca et al., 2009).

1.3.2. Mitochondrial dynamics and quality control

As the most important powerhouse of eukaryotic cells, mitochondria have developed many strategies to maintain their functions through mitochondrial quality control. Under the regulation of various quality control proteins, slightly damaged mitochondria can be repaired by fusion with healthy mitochondria and mixing the content, while severe damaged mitochondria are removed by mitophagy or can induce cell apoptosis (Tatsuta and Langer, 2008). Mitochondrial dynamics involves the fusion and fission processes of mitochondrial membrane and reflects mitochondrial morphology of the cell. It is a vital mechanism for mitochondrial quality control regulated by dynamin-related GTPase machineries, including MFN1, MFN2, OPA1 and DRP1 in mammals (Detmer and Chan, 2007).

Mitofusins MFN1 and MFN2, located in mitochondrial outer membrane, regulate the mitochondrial membrane fusion reaction (Chen et al., 2003). The inner membrane protein Optic atrophy 1 (OPA1), which has several splice variants, also regulates mitochondrial membrane fusion (Lee et al., 2004; Song et al., 2007) and cristae structure remodeling (Frezza et al., 2006). On the contrary, DRP1 controls the mitochondrial fission progress (McBride et al., 2006). Both of the mitochondrial dynamic processes are essential for cells. Mitochondrial fusion is an efficient way to replace mutant mtDNA and compensate damaged components in dysfunctional mitochondria, while mitochondrial fission lead to segregation and autophagy of irreparable mitochondria. Disruption of these regulatory proteins for mitochondrial

dynamics is associated with cellular dysfunction and predisposition to diseases. For example, knockout of *MFN1* and *MFN2* genes in mouse embryonic stem cells leads to lethality (Chen et al., 2003), and mutated *MFN2* is correlated with Charcot-Marie-Tooth disease (CMT) (Züchner et al., 2004). Patients carrying *OPA1* mutations commonly have multi-system neurological disorders (Yu-Wai-Man et al., 2010), such as the dominant optic atrophy notably (Delettre et al., 2000; Alexander et al., 2000). The aberrant interaction between DRP1, amyloid beta and phosphorylated tau has been associated with Alzheimer's disease (Manczak and Reddy., 2012).

1.3.3. Loss of *AFG3L2* gene causes OPA1 protein cleavage and mitochondrial fragmentation

OPA1 is a dynamin-related GTPase that controls mitochondrial fusion by proteolytic cleavage. In human, 8 mRNA variants were found by alternative splicing during *OPA1* gene transcription (Delettre et al., 2001). These different mRNA splice forms produce two types of protein isoforms: one long isoform (L-OPA1) and several short isoforms (S-OPA1). Both OPA1 isoforms work corporately to support mitochondrial fusion (Song et al., 2007). Remarkably, the destabilization of L-OPA1 results in OPA1 processing and loss of protein activity, thus causing mitochondrial fragmentation.

The m-AAA metalloprotease regulates the OPA1 processing. Loss of *AFG3L2* gene can significantly decrease the stability of L-OPA1 in human cells and stimulate the cleavage of OPA1 by OMA1, which is also a metallopeptidase similar to m-AAA metalloprotease (Ehses et al., 2009). Higher cell percentage of fragmented mitochondria was observed in dominant-negative AFG3L2 variant human cells than in normal cells (Ishihara et al., 2006). Additionally, respiratory dysfunction and mitochondrial Ca^{2+} uptake are also consequences of AFG3L2 deficiency (Maltecca et al., 2012). Neuroscience studies have indicated that dysfunction of *AFG3L2* gene is predisposed to neurodegenerative disorders such as SCA28 (Di Bella et al., 2010) and spastic ataxia-neuropathy syndrome (Pierson et al., 2011). According to these facts,

we believe that knocking down of *AFG3L2* gene in human cells may lead to an in vitro disease model for imitating neurodegenerative diseases.

1.4. Alternative pathway for compensating respiratory chain defects

Apart from the classical respiratory chain complexes, scientists have also found alternative enzymes that are involved in mitochondrial electrons transportation. These enzymes exist in many organisms, such as fungi, microbes, plants and certain animal phyla. The NADH dehydrogenase (Ndi1) makes *Saccharomyces cerevisiae* insensitive to rotenone by replacing complex I functionally (Matus-Ortega et al., 2015). The alternative oxidase (AOX) confers cyanide-resistance to lower animals such as *Ciona intestinalis* and *Crassostrea gigas* (McDonald et al., 2004). These enzymes can provide an alternative pathway for electrons to pass through the blocked respiratory chain, thus protecting the organism under unfavorable conditions. Although alternative enzymes are not found in arthropods and mammalians, they show no detrimental phenotype when expressed in drosophila (Fernandez-Ayala et al., 2009) and mouse models (El-Khoury et al., 2014). Therefore, we see the alternative enzyme as a new therapy for mitochondrial diseases from the aspect of rescuing the mitochondrial respiratory chain.

1.4.1. Function and application of alternative oxidase

The alternative oxidase (AOX) is a membrane-bound enzyme that transfers electrons from ubiquinone pool to convert the oxygen into water, bypassing the cytochrome c pathway of the respiratory chain (see Fig 2). This enzyme was first found in the study of thermogenic bloom in aroids (Meeuse, 1975), AOX helps flowers produce heat to spread scent so as to attract insects for pollination. As a terminal oxidase of many plants, AOX also enables the mitochondria to tolerate certain toxins such as cyanide. In the presence of cyanide, cytochrome c oxidase fails to pass electrons to oxygen

through the mitochondrial respiratory chain, leading to excessive ROS and failure of ATP production. However, AOX makes the mitochondria insensitive to cyanide as it can transport electrons from substrates to oxygen by itself. Interestingly, the activity of AOX is usually maintained at low level unless the traditional respiratory chain is inhibited or blocked, which can stimulate the AOX activity (Rogov et al., 2014). The alternative pathway provided by AOX seems like a compensational oxidative mechanism under stress conditions such as oxidative stress, temperature changes, drought, nutrients shortage and so on, increasing the metabolic flexibility of cells. Besides plants, AOX was also found in yeast, fungi, protist, algae (McIntosh, 1994), and lower invertebrate animals such as *Ciona Intestinalis* (McDonald et al., 2004).

However, *AOX* gene no longer exists in vertebrates, probably due to gene loss event during the evolution (McDonald et al., 2009). AOX protein has been applied in several animal models for studying its expression and function in mitochondria. Drosophila engineered to express AOX ubiquitously, showed antimycin and cyanide resistance of mitochondria, along with rescued function of oxidative phosphorylation in mutated cytochrome chain (Fernandez-Ayala et al., 2009). Studies have further supported the therapeutic function of AOX by the alleviation of defective phenotypes in the drosophila which had cytochrome oxidase deficiency (Kemppainen et al., 2014) and increased lifespan of the drosophila that produced human beta-amyloid in neurons (El-Khoury et al., 2016). Similar results were observed in mouse models as well. The expression of AOX in the transgenic mice reduced the ROS production and maintained the electron flow in the blocked mitochondrial respiratory chain (El-Khoury et al., 2013). Better still, AOX affects no normal physiology of the transgenic mice (Szibor et al., 2017). Moreover, scientists also applied AOX to human cells to study the mitochondrial respiratory chain defects and found its therapeutic potential on mitochondrial diseases (Hakkaart et al., 2006; Dassa et al., 2009).

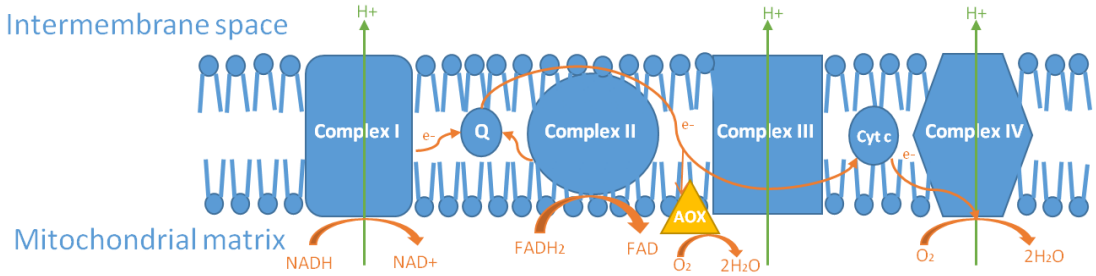

Fig 2. AOX provides an alternative way for electrons flow in the respiratory chain

In the presence of AOX (*yellow triangle*), the electrons transferred from ubiquinone (Q) can bypass the traditional respiratory chain and directly reduce the oxygen to produce water. However, AOX helps nothing in proton pumping across the mitochondria membrane and generates no energy.

1.4.2. Regulation of AOX activity

The activity of AOX is widely regulated by both genetic and epigenetic factors. Different transcription factors control the AOX expression in different species. *Arabidopsis thaliana* has a variety of transcription factors that affect AOX expression, including ABI4 (Giraud et al., 2009), NAC factors (Clercq et al., 2013) AtWRKY40 and AtWRKY63 (Aken et al., 2013). While *aod-2, aod-4, aod-5, aod-6, aod-7* genes regulate the AOX expression in fungi (Rogov et al., 2014). In addition to genetic factors, substrates involved in the respiratory chain can also regulate AOX activity at posttranslational level. Pyruvate is a common substrate that activates the AOX function. Whereas in some isoenzymes of sacred lotus, the AOX activity is insensitive to pyruvate but can be enhanced by succinate (Grant et al., 2009). In fungi and yeast, purine mono- or diphophates activate AOX in the presence of substrates (Sierra-Campos et al., 2009).

As mentioned in 1.4.1, the regulation of AOX activity also depends on stress conditions. Disruption of the mitochondrial respiratory metabolism is one of the critical reasons to induce the expression of AOX in mitochondria. A sharp increase of AOX expression was observed in tobacco when antimycin A inhibited the cytochrome pathway (Vanlerberghe et al., 1994), leading to significant respiration in the

alternative pathway. Analogous results were also found when citrate, acetate, H_2O_2, or cysteine was introduced to the tobacco cell, meaning that AOX can be upregulated by multiple metabolites and stresses (Vanlerberghe et al., 1996). Further study regarding Arabidopsis suggested that the expression level of AOX also varied from tissues and developmental stages based on different genotypes from the same gene family (Clifton et al., 2006).

On the other hand, AOX has its specific inhibitors. N-propyl gallate (nPG) and salicyclhydroxamic acid (SHAM) are two common inhibitors that efficiently inhibited the cyanide-resistant oxygen consumption in Plasmodium falciparum (Murphy et al., 1997). These inhibitors shut down the alternative electron transportation pathway provided by AOX, forcing the electrons in mitochondrial membrane to pass the cytochrome c pathway merely. Because of this function, SHAM and nPG are widely used to eliminate the impact of AOX on mitochondrial respiration.

1.5. Viral vector as a tool to express AOX gene in mammalian cells

On account that AOX protein is absent in mammals, the recombinant DNA technology can be applied to express the AOX gene of *Ciona intestinalis* in mammalian cells or tissues. An engineered double-stranded circular DNA, known as plasmid, is the basic component for accomplishing this goal. Plasmids are commonly found in bacteria such as E. coli. These small circular DNA carry different genes than the chromosome and can replicate independently, which makes them ideal vectors for gene cloning. Usually, recombinant plasmids have gene markers that express antibiotic resistance, allowing for screening of positive clones subsequently. Plasmids can transfer the gene of interest directly into the target cells by transfection, or proliferate the gene in competent bacteria by transformation. The gene delivered by plasmid transfection can only be expressed transiently in host cells, because the genome of host will not integrate the plasmid gene. However, Ti plasmid of

Agrobacterium tumefaciens is an exception, which can insert the foreign gene from T-DNA region of plasmid into plant genome (Stachel aandNester, 1986).

Due to the limitation of plasmid transfection, a more stable vector has been established in many research fields, that is the virus. There are a variety of viral vectors capable for delivering exogenous gene into host cells, some can even integrate the carried gene into the genome of the host. Each of these viruses has different advantages and drawbacks. But they generally own predominant qualities such as less cytotoxic, genetically stable, and highly flexible for various cell types. Four types of most commonly used viral vectors are listed in Table 1.

Compared with all the characteristics of other viral vectors, the lentivirus is more advantageous for stably expressing AOX in the human cells that divide slowly. Efficient transfer ability and sustained gene expression of lentiviral vectors have been observed in rodent tissue, HEK293T cells (Naldini et al., 1996), U2OS cells (Stegmeier et al., 2005), and human fibroblasts (Mali et al., 2008). To improve the safety of lentivirus packaging, separated plasmids that contain different viral genes were generated as the 3rd generation lentivirus packaging system (Dull,T et al., 1998). In this system, two packaging viral vectors and one envelop vector are co-transfected along with the recombinant plasmid into cells, so that intact viruses can be integrated in the cells and released into the cell culture medium. By this method, transgenic lentiviruses are produced but with loss of the ability to proliferate uncontrollably.

	Adenovirus	Adeno-Associated virus	Retrovirus	Lentivirus
Virus gene size	36kb	8.5kb	7-11kb	8.5kb
Insert gene size	8kb	5kb	8kb	9kb
Gene type	dsDNA	ssDNA	ssRNA	ssRNA
Gene integration	No	Yes (specific site)	Yes	Yes
Efficiency	High	High	Medium	Medium
Target cell	Dividing and non-dividing	Dividing and non-dividing	Dividing	Dividing and non-dividing
Disadvantage	Strong immune response	Require helper virus to replicate, hard to	Host cell mutagenesis	Host cell mutagenesis

		guarantee purity	potential	potential

Table 1. Comparison of four common viral vectors (adapted from Thermo fisher scientific)

The table lists the virus gene size, insert gene capacity, gene type, gene integration, infection efficiency, target cell and disadvantages of four common viral vectors. One can choose the most suitable vector depending on the purpose of experiment and essential features of each vectors.

1.6. Aim of study

Although being underestimated by many people, mitochondrial diseases are among the most important diseases that significantly threaten human health. Especially the dysfunction of mitochondria in the brain, since brain is the most energy dependent organ, leads to various neurodegenerative diseases which lack of efficient treatments. Despite huge challenges, scientists are actively exploring potential therapies to conquer these stubborn diseases.

As introduced previously, AOX has the beneficial characteristic to compensate the defects in the mitochondrial respiratory chain by providing an alternative electron pathway and alleviating the excessive oxygen stress. Hence we see AOX as a promising candidate to cure mitochondrial diseases. Considering that AOX is absent in human, we established a transgenic mouse model to express *Ciona AOX* gene ubiquitously in the animal for our study (Szibor et al., 2017). However, by comparing the expression level of AOX protein in different tissues of the transgenic mouse model, we found that AOX was expressed surprisingly lower in the brain than heart or any other tissues (see Fig 3).

To explore how this happened and define the real function of AOX in the brain, both at tissue level and cell level, we started our study on this transgenic mouse model from two aspects. On one hand, we aimed at confirming the preliminary results of AOX expression in the mouse brain with more samples and different tissue extraction methods. In addition, we were also interested in the expression level of AOX in the isolated neuro-glia cells. On the other hand, we aimed at constructing a recombinant

viral vector to induce the expression of AOX in wild type mice and human cell lines, further investigating the AOX function under disease conditions. For example, we built an in vitro disease model that mimicked a type of neurodegenerative disease related to mitochondrial dysfunction, and the viral vector could be applied to this disease model to test whether AOX can alleviate any symptoms caused by mitochondrial defects.

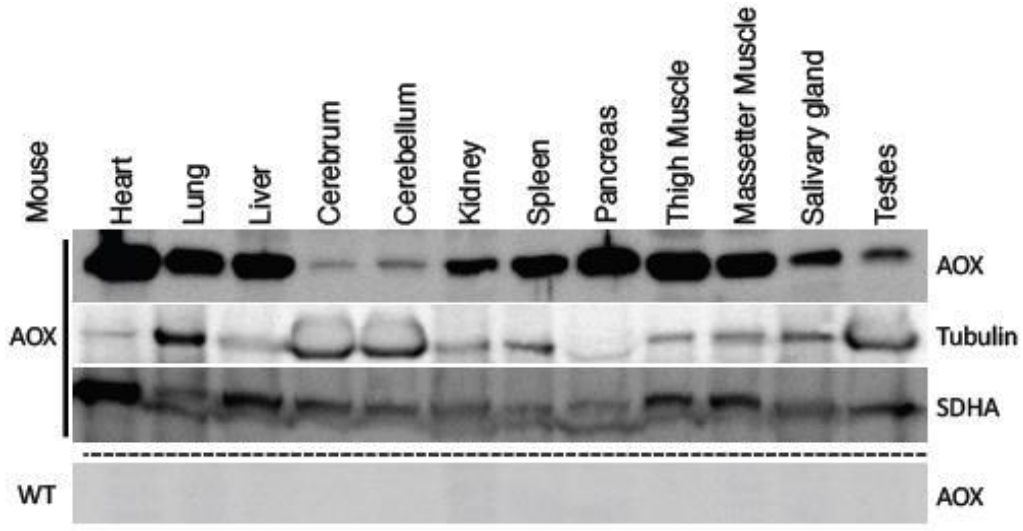

Fig 3. AOX expression in different mouse organs

Western blots of 20μg total tissue protein extracted from hemizygous *AOX*^{Rosa26} transgenic mice and wild type mice were probed with AOX, tubulin and SDHA antibodies separately. Blots show relatively low expression of AOX protein in cerebrum and cerebellum compared with other tissues (Szibor et al., 2017).

2. Material and method

2.1. Materials

2.1.1. Mouse model

The *AOX*^{Rosa26} transgenic mouse model was generated from the mouse embryonic stem cell (Srinivas et al., 2001), in which the *AOX* gene from *Ciona intestinalis* was knocked into the *Rosa26* gene locus (Friedrich and Soriano, 1991; Szibor et al., 2017).

The *AOX* transgene was expressed all over the body of the transgenic mouse driven by *CAG* promoter (Hitoshi et al., 1991). And the AOX^{Rosa26} transgenic mouse line was maintained by backcrossing to strain C57Bl/6J and mating between littermate siblings. The genotype of each mouse was checked consistently by PCR.

2.1.2. Chemicals and solution

2.1.2.1 Western blotting buffers

12% Separating gel (5ml)

The gel was made by mixing 1.6ml of distilled water, 2ml of 30%Acrylamide/Bis solution (BIO-RAD #1610156), 1.3ml of 1.5M Tris-HCL (pH 8.8), 25µl of 20% SDS, 50µl of 10% APS and 2µl of TEMED (BIO-RAD #1610800) until the gel was polymerized.

Stacking gel (2ml)

The gel was made by mixing 1.4ml of distilled water, 330µl of 30%Acrylamide/Bis solution (BIO-RAD #1610156), 250 µl of 1.0M Tris-HCL (pH 6.8), 10µl of 20% SDS, 20µl of 10% APS and 2µl of TEMED (BIO-RAD #1610800) until the gel was polymerized.

SDS-PAGE running buffer

1x running buffer was prepared by diluting 10x stock (purchased from Institute of Biotechnology Media Kitchen) 1 in 10 with distilled water. The 10x stock contains 3% Tris, 14.4% glycine and 1% SDS in Mili-Q water.

5x Laemmli buffer

The buffer was made by dissolving 0.312M Tris-HCL (pH 6.8), 10% SDS, 50% glycerol, 25% β-Mercaptoethanol and 0.05% bromophenol blue in distilled water.

Semidry transfer buffer

The buffer purchased from Institute of Biotechnology Media Kitchen contains 0.3%

Tris, 1.44% glycine and 20% methanol in Mili-Q water.

TBST (Tris buffered saline/0.1% Tween 20) buffer

The buffer was diluted from 10x TBS pH=7.4 (purchased from Institute of Biotechnology Media Kitchen) with 0.1% of Tween 20. 10x TBS contains 3% Tris, 8% NaCl, 0.2% KCl in Mili-Q water.

Blocking buffer

The buffer was prepared by dissolving 1.5% (w/v) non-fat milk powder in TBST.

Western Blot stripping solution

The solution was made by mixing 100mM β-Mercaptoethanol, 2% SDS, 62.5mM Tris-HCL (pH 6.8) in distilled water.

Primary antibody solution

AOX [customized rabbit antibody, 21st Century Biochemicals (Fernandez-Ayala et al., 2009)], dilution ratio was 1:50000 or 1:10000

α-tubulin (Cell Signaling Technology #3873), dilution ratio was 1:2000

GAPDH (Cell Signaling Technology #5174), dilution ratio was 1:1000

SDHA (Abcam #ab14715), dilution ratio was 1:10000

AFG3L2 (Proteintech #14631-1-AP), dilution ratio was 1:5000

OPA1 (BD Biosciences # 612606), dilution ratio was 1:10000

The antibodies were diluted in the TBST solution containing 5% bovine serum albumin (protease free BSA, Jackson ImmunoResearch #001-000-162).

Secondary antibody solution

Anti-rabbit (Jackson ImmunoResearch #111-035-144), dilution ratio was 1:20000

Anti-mouse (Jackson ImmunoResearch #115-035-146), dilution ratio was 1:10000

The antibodies were diluted in TBST.

Luminol chemiluminescent solution

The luminol chemiluminescent substrates were mixed from 20x LumiGLO Reagent

and 20x Peroxide (Cell Signaling Technology) and diluted in water according to the manufacturer's recommendations.

2.1.2.2 Protein extraction buffers

1xPBS (Phosphate-buffer saline) buffer

The buffer purchased from Institute of Biotechnology Media Kitchen contains 0.8% NaCl, 0.02% KCl, 0.14% Na_2HPO_4 x $2H_2O$, 0.02% KH_2PO_4 in Mili-Q water.

10xPBS buffer

The buffer purchased from Institute of Biotechnology Media Kitchen contains 8% NaCl, 0.2% KCl, 1.4% Na_2HPO_4 x $2H_2O$, 0.2% KH_2PO_4 in Mili-Q water.

Tissue lysis buffer

The buffer contains 50mM Tris-HCL (pH 7.5), 150mM NaCl, 1mM EDTA, 1% Triton, 2.5mM PMSF and Pierce protease inhibitor tablet (Thermo Fisher Scientific) dissolved in Mili-Q water.

Cell lysis buffer

The buffer was made by dissolving 1%DDM (N-Dodecyl-2-D-Maltoside), 1mM PMSF (Phenylmethanesulfonyl fluoride solution) and one tablet of Pierce protease inhibitor (Thermo Fisher Scientific) in 10ml 1xPBS.

RIPA buffer (Sigma #R0278)

The buffer contains 150mM NaCl, 1%IGEPAL® CA-630, 0.5% sodium deoxycholate, 0.1% SDS, and 50 mM Tris, pH= 8.0.

2.1.2.3 Cell culture solutions

FBS (Fetal Bovine Serum) solution

The stock solution (Thermo Fisher Scientific #10270106) was inactivated in 56^{o}C water bath for 30min and aliquoted in -20^{o}C freezer before use.

DMEM complete medium

The medium was made by adding 10% FBS, 1% GlutaMAX™ Supplement (Thermo Fisher Scientific #35050038) and 1% Pen/Strep (Lonza #DE17-602E) in high glucose DMEM medium (Lonza #BE12-614F).

DMEM galactose medium (no glucose)

The medium was made by adding 1% Pen/strep (Lonza #DE17-602E), 1% 100mM sodium pyruvate solution (Sigma #S8636), 10mM Galactose, 10% FBS in DMEM no glucose medium (Thermo Fisher Scientific #11966025, with L-glutamine).

Neurobasal A complete medium

The medium was made by adding 1% Pen/strep (Lonza #DE17-602E), 1% GlutaMAX™ Supplement (Thermo Fisher Scientific #35050038) and 10% B-27™ Supplement (Thermo Fisher Scientific #17504044) in CTS™ Neurobasal™-A Medium (Thermo Fisher Scientific #A1371001)

0.0025% PDL (Poly-D-lysine)

The solution was made by dissolving PDL powder (Sigma #P7280) in distilled water.

0.01%PLL (Poly-L-Lysine)

The solution was made by dissolving PLL powder (Sigma #P2636) in distilled water.

0.25% Trypsin (no EDTA) solution

The solution was prepared fresh by diluting Trypsin Solution (2.5%) 10X (Sigma #59427C) in PBS.

0.05% Trypsin-EDTA solution

The solution was diluted from Trypsin-EDTA (0.5%) Solution 10X (Thermo Fisher Scientific #15400054) in PBS.

Antimycin A solution

The solution was made by dissolving Antimycin A from Streptomyces sp. (Sigma

#A8674) in pure ethanol.

2.1.2.4 Transfection solutions

5x KCM buffer

The buffer contains 500mM KCL, 150mM $CaCl_2$ and 250mM $MgCl_2$ in sterile water.

LB medium

The medium purchased from Institute of Biotechnology Media Kitchen contains 1% tryptone, 0.5% yeast extract and 0.5% NaCl in Mili-Q water.

Lipofectamine 2000 transfection reagent (Invitrogen #11668019)

Lipofectamine RNAiMAX transfection reagent (Invitrogen #13778030)

Opti-MEM reduced serum medium (Invitrogen #31985062)

siRNA

Stealth RNAi™ siRNA Negative Control (Invitrogen #12935300)

Human AFG3L2 stealth siRNA (Invitrogen #HSS116886)

2.1.2.5 Oxygraph solutions and immunostaining buffers

Mitochondrial respiration medium (MiR05)

The buffer was made of 0.5mM EGTA, 3mM $MgCl_2$, 60mM lactobionic acid (Sigma #153516, pH adjusted to 7.0 with 5M KOH), 20mM taurine (Sigma #T0625), 10mM KH2PO4, 20 mM HEPES/KOH, 110mM sucrose and 1mg/ml fatty-acid free BSA (Sigma #A7030), pH was adjusted to 7.2 at room temperature.

Mitochondrial extraction buffer

The buffer was made of 225mM sucrose, 75mM D-mannitol, 10mM Tris base, 1mM EGTA, and 1mg/ml fatty-acid free BSA in H_2O, pH was adjusted to 7.4 with HCL.

Rotenone solution

The solution was made by dissolving rotenone powder (Sigma #R8875) in pure ethanol.

4% PFA buffer

4% Paraformaldehyde powder (Sigma #158127) was dissolved in Mili-Q water by water bath and 10x PBS buffer was diluted into 1x PBS with the dissolved paraformaldehyde solution. Final pH was adjusted to 7.2 by pH meter. The buffer was filtered by a falcon cell strainer (Thermo Fisher Scientific #08-771-1).

PBST buffer

The buffer was made by adding 0.1% of Tween 20 into 1x PBS buffer.

2.2. Methods and techniques

2.2.1. Genotyping and gel electrophoresis

DNA samples were extracted from ear punches or tail snips of the mice by AccuStart™ II Mouse Genotyping Kit according to manufacturer's instructions. Genotypes were verified by PCR using AccuStart II GelTrack PCR SuperMix (2X) with primers AOX 317F (5'-GCGATGCAAGATGGAGGGTA-3') and AOX 317R (5'-TGAATCCAACCGTGGTCTCG-3'), plus Rosa26_wt_gtF (5'-GACCTCCATCGCGCACTCCG-3') and Rosa26_wt_gtR (5'-CTCCGAGGCGGATCACAAGC-3'). All the primers were ordered from Sigma. The PCR was performed in a thermal cycler with the final reaction volume of 25μl, including 1μl of extracted DNA sample, 0.16μM of each primer, 12.5μl of the AccuStart II GelTrack PCR SuperMix (2X). The PCR thermal cycling condition was set up as follows: initialization for 3min at 95^{o}C, denaturation for 20s at 95^{o}C, annealing for 30s at 56^{o}C, extension for 40s at 72^{o}C, repetition for 35 cycles, and final elongation for 8min at 72^{o}C. PCR products were separated in a 1% agarose gel, at 90V for 1h.

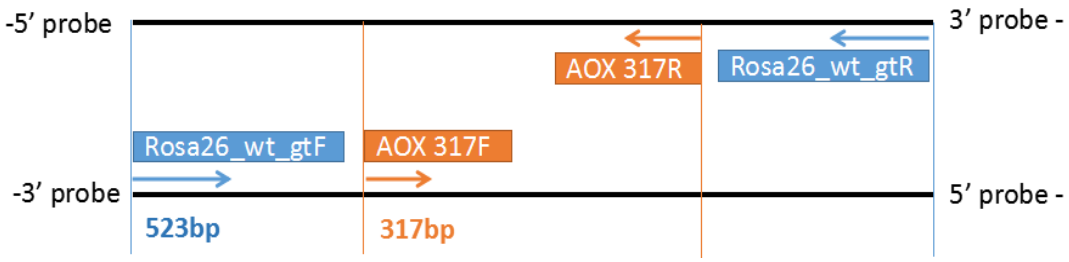

Fig 4. AOX gene location and primers design

In the genome of the *AOX*^{Rosa26} transgenic mouse model, *Ciona AOX* gene (*orange*) is inserted into the *Rosa26* gene sequence (*blue*). The sizes of PCR product amplified by *AOX* primers and *Rosa26* primers are 317bp and 523bp, respectively.

2.2.2. Protein extraction

2.2.2.1. Protein extraction from the cell

Cultured cells were washed with PBS and removed from the plate by a scraper or 1x trypsin solution (trypsinized the cell for 5min at 37^{o}C). Cells were further centrifuged for 5min at 400xg to discard the supernatant, and cell pellets were resuspended in cell lysis buffer. After 30min of incubation on ice, the protein lysate was separated from the cell residue by centrifugation for 15min at 20000xg, 4^{o}C.

2.2.2.2. Protein extraction from the tissue

200µl tissue lysis buffer was added for 20-30mg tissue and homogenized on ice with scissors and pestles. Tissue lysate was incubated on ice for 30min and centrifuged for 5min at 14000xg, 4^{o}C.

2.2.2.3. Measurement of protein concentration

Protein concentration was estimated by Bradford assay (Bradford, 1976) using diluted Bio-Rad Protein Assay Dye Reagent Concentrate (Bio-rad #5000006) and a microplate reader (SpectraMax 190, Molecular Devices). 0, 1, 2, 4, 8 mg/ml of BSA were used to prepare the standard gradient.

2.2.3. Western blotting

2.2.3.1. Customized gel protocol

Protein samples were diluted to the same concentration, mixed with 5x laemmli buffer and loaded into the SDS-PAGE self-made gel for electrophoresis. The self-made gel was made of 2 layers, including a 12% polyacrylamide gel and a stack gel. The electrophoresis was carried out in a SDS-PAGE running chamber (Bio-rad) for 1.5h at 100V. Separated proteins were transferred from the gel to a PROTRAN nitrocellulose membrane in the Owl™ HEP-1 Series Semidry Electroblotting Systems (Thermo Fisher Scientific) for 1h at 0.04A, at room temperature. The western blot membrane was then blocked with blocking buffer (1.5% milk in TBST), and incubated with primary antibody solution overnight at 4^{o}C. Next day, the membrane was washed in TBST (10min for each wash, repeated 3 times) and probed by peroxidase-conjugated secondary antibody for 1h at room temperature. After the same washing steps as before, the membrane was soaked in the luminol chemiluminescent solution for 3 min and detected by a ChemiDoc XRS Imaging System.

2.2.3.2. Commercialized gel protocol

In this protocol, the self-made gel was replaced by a 4–20% Mini-PROTEAN® TGX™ Precast Protein Gel (Bio-rad #4561093). A Trans-Blot® Turbo™ Mini PVDF Transfer Pack (Bio-rad #1704156) was used for the semidry transfer blotting in a Trans-Blot® Turbo™ Transfer System (Bio-rad). The 1 mini gel TGX programme was selected for the transfer system according to manufacturer's instructions. The PVDF membrane was further treated and detected as the same as in 2.2.3.1.

2.2.3.3. Stripping

Stripping steps were implemented when more than one primary antibodies needed to

be blotted. The stripping buffer was prewarmed to 56^{o}C before stripping. Membranes were stripped for 30min at room temperature and washed twice in TBST buffer, each wash lasted for 15min. Antibody was added to the membrane after 30min of blocking with blocking buffer.

2.2.4. Cell culture

2.2.4.1. Cell line maintenance

Primary neuro-glia cell

To separate neuro-glia cells from the mouse brain, the cortex was collected from the cervical dislocated mice and cut into pieces with scissors in PBS. The brain pieces were trypsinized for 5min at 37^{o}C and further triturated in DMEM complete medium. The triturated brain cells were resuspended in DMEM before plating onto 6 well cell culture plate, which was coated by 0.0025%PDL in advance. The cells were first cultured in DMEM complete medium for 1 day and then changed to neurobasal A complete medium with all the cell debris cleaned out. The incubation condition was 37^{o}C with 5% CO_2.

HEK293T cell

The cell line was cultured in DMEM complete medium. Medium was changed every 3 days. And cells were subcultured when cell confluence reached 100%. 4x10^{6}/ml of cells were frozen in FBS solution with 10% DMSO (Sigma #D2650) for preservation.

U2OS

The cell line was cultured in DMEM complete medium. Medium was changed every 3 days. And cells were subcultured when cell confluence reached 100%. One full confluent 10cm^{2} plate of cells were frozen in FBS solution with 10% DMSO (Sigma #D2650) for preservation.

2.2.4.2. Antimycin A treatment

The neuro-glia cells were cultured in DMEM complete medium for 1 day, and in neurobasal A complete medium for 2 days before the treatment. Cells were washed with PBS once and cultured in DMEM galactose medium (no glucose) for antimycin A treatment. Different amount of antimycin A solution was added to each well of 6 well cell culture plate and cell viability was recorded under the inverted microscope (Leica DMi1) with a camera after 24h of treatment.

2.2.4.3. Plate coating

The plates should be coated before primary neuro-glia cell culture and HEK293T cell transfection. For neuro-glia cell culture, 1ml of 0.0025%PDL solution was used to coat each well of 6 well cell culture plate for 5min, and the solution was washed away by sterile water for 3 times. 1ml of DMEM complete medium was added to each well when the plate was completely dry. The plate was incubated at 37^{o}C before use. For HEK293T cell transfection, 10ml of 0.01%PLL solution was used to coat 10 cm^{2} plate for 5min, followed by the same washing and drying steps as PDL, and 37^{o}C DMEM complete medium was added to the plate before introducing cells.

2.2.5. Mitochondrial respiration

2.2.5.1. Mitochondrial extraction

Mice were sacrificed by cervical dislocation for mitochondrial extraction. Tissues collected from the mice were chopped into pieces of 2mm^{3} in ice-cold PBS and further into 1mm^{3} in 3ml of ice-cold mitochondrial extraction buffer by scissors. Tissue pieces were homogenized in mitochondrial extraction buffer by stroking 5-6 times with a pestle in a glass-teflon homogenizer on ice. The homogenate was transferred to a 15ml falcon tube and centrifuged at 1300xg for 5min at 4^{o}C. The supernatant of the homogenate was collected and re-centrifuged at 17000xg for 15min

at 4°C. Mitochondrial pellet was resuspended in ice-cold MiR05 buffer (protease inhibitor added) before the respirometry. The concentration of mitochondria was measured using Bradford assay (Bradford, 1976).

2.2.5.2. Mitochondrial respirometry

The mitochondrial oxygen consumption was measured by a high-resolution respirometry: oxygraph-2k (OROBOROS Instruments, Austria). Respiratory chambers of the oxygraph were washed thoroughly 3 times with 70% ethanol and 3 times with Mili-Q water. A calibration of the polarographic oxygen sensor was performed before the experiment following the manufacturer's protocols (Pesta and Gnaiger, 2012). 50 or 100µg of mitochondria were added to each respiratory chamber which contained 2.2ml of MiR05 buffer. After 5min of equilibrium, following substrates and inhibitors were added to each chamber in order: (1) 5mM of sodium pyruvate, 5mM of sodium glutamate and 5mM of sodium malate, (2) 2mM of ADP, (3) 150nM of rotenone, (4) 17mM of sodium succinate, (5) 22.5ng/ml of antimycin A, (6) 250µM of n-propyl gallate (nPG), (7) 0.5mM of N,N,N',N'-tetramethyl-p-phenylenediamine (TMPD) plus 2mM of sodium L-ascorbate, (8) 50mM of sodium azide. The oxygen flux in each respiratory chamber was recorded by DatLab software simultaneously. The flux values were normalized according to the amount of mitochondria and analyzed with Microsoft Excel software.

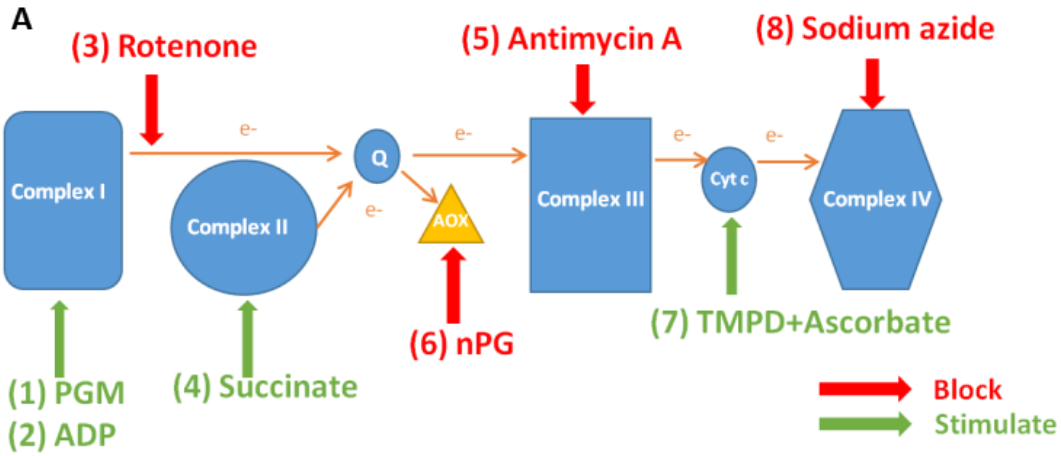

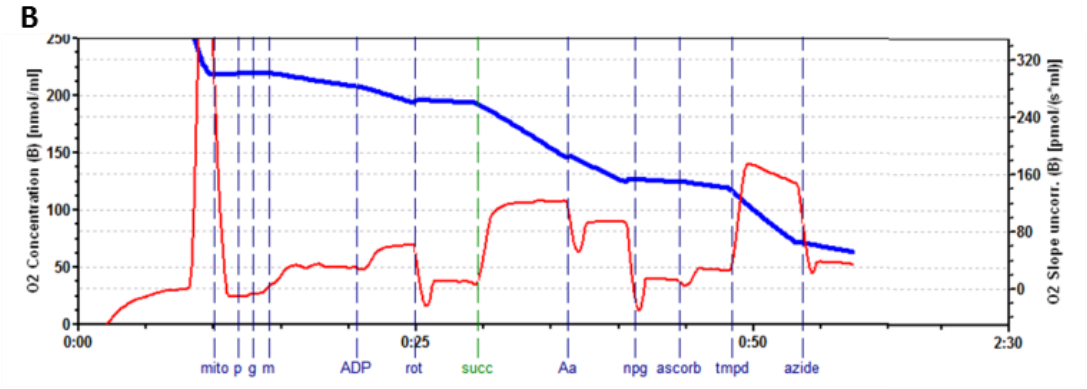

Fig 5. Respirometry process

(A) The process of respirometry. Red chemicals represent the inhibitors of specific complexes or enzyme. Green chemicals represent the substrates of those complexes. Pyruvate, sodium glutamate and sodium malate are abbreviated as P, G, M. (B) A representative oxygen consumption graph of oxygraph-2k, which shows the adding order of specific chemicals after the mitochondria have been added into the respiratory chamber, as well as how the oxygen concentration (blue bar, value on the left y-axis) and oxygen slope (red bar, value on the right y-axis) change during the whole process.

2.2.6. Construction of AOX lentiviral vector

2.2.6.1. Plasmid construction

A pCDH-IRES-EGFP plasmid ordered from Systems biosciences was used as the backbone for our target plasmid. To insert *Ciona AOX* gene into the plasmid, the restriction enzymes EcoRI and NotI were used for digestion. 5µl plasmid DNA (plasmid concentration was 1-2µg/µl) was incubated with 10U of each enzyme in 50µl reaction system with FastDigest buffer (Thermo Fisher Scientific #B64) for 1h at 37^{o}C. After the gel electrophoresis of the digested plasmid, the backbone DNA was collected under UV light and extracted by a NucleoSpin Gel and PCR clean-up kit (Macherey-Nagel #740609). 11µl transgene and 5µl plasmid backbone were rejoined by 1µl T4 DNA ligase (Thermo Fisher Scientific #EL0011) in 20µl reaction system with ligase buffer for 2h at 16^{o}C.

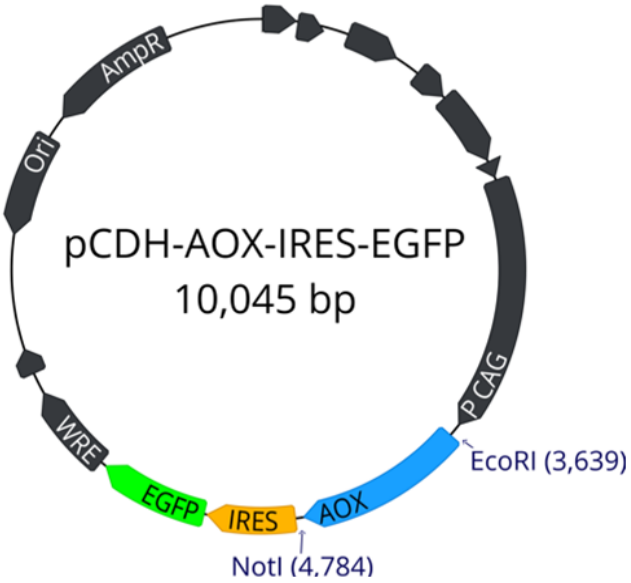

Fig 6. AOX plasmid construct

The recombinant AOX plasmid of 10,045 bp contains the replication origin (*Ori*), the antibiotic marker of ampicillin (*AmpR*), the synthetic promoter (*pCAG*), the *Ciona AOX* gene, the internal ribosome entry site (*IRES*), the enhanced green fluorescent protein gene (*EGFP*), the Woodchuck hepatitis virus Post-transcriptional Regulatory Element (*WRE*) and the restriction sites *EcoRI* and *NotI*.

2.2.6.2. Transformation

5-50µg recombinant plasmid and 10µl 5X KCM buffer were added to 50µl chemically competent *E. coli* in 100µl reaction system. The mixture was incubated first on ice for 20min and then at room temperature (RT) for 10min, after which 1ml of LB medium was added to it and altogether incubated for 1h at 37^{o}C, 750 rpm. The transformed *E. coli* were spread on a LB agar plate with ampicillin and incubated at 37^{o}C overnight.

2.2.6.3. Amplification and purification of plasmid DNA

Four random single colonies were picked from the LB agar plate and inoculated in 3ml LB medium with ampicillin (50µg/ml) separately. The bacteria were incubated at 37^{o}C overnight at 220rpm.

2ml of the LB culture was used for a minipreparation (miniprep) of plasmid DNA on the next day. The miniprep was accomplished with a NucleoSpin Plasmid Kit

(Macherey-Nagel #740588), according to manufacturer's instructions. The purified DNA was digested with restriction enzymes EcoRI and NotI and separated on a 1% agarose gel. Correct plasmid was verified by the size of insert gene.

Plasmid of the right size was further amplified by midipreparation (midiprep) using a NucleoBond Xtra Midi kit (Macherey-Nagel #740410) according to manufacturer's instructions.

2.2.6.4. Viral vector production

5×10^6 HEK293T cells (Passage<20) were seeded in a 10 cm^2 PLL coated plate with 10ml DMEM complete medium. Cells were split 1:8 to 3 plates if they reached 90% confluency, and the supernatant was collected for ultracentrifugation to concentrate the virus. Cell confluency of each plate should be 70% before transfection.

In a 500µl transfection system, 7µg of transfer plasmid and 3.5µg of each packaging plasmid, including pRRE, pRSV and pMD2.G, was pre-mixed with 250µl of 150mM NaCl, while 36µl of jetPEI transfection reagent (Polyplus #101-10N) was pre-mixed with 250µl of 150mM NaCl. After 5min of incubation at RT, two parts of solution were combined together and mixed gently. The DNA-jetPEI complex was dropwise added to HEK293T cells in the $10cm^2$ plate after 20min of incubation at RT. The transfected cells were incubated at 37°C. 4h later, the cell culture medium was changed with 10ml of fresh DMEM complete medium.

The supernatant containing virus was collected and filtered with a 0.45µm PES filter into 50ml falcon tube after 48-72h of cell culture. The virus could be used fresh or concentrated with an ultracentrifuge at 22000rpm for 2h at 4°C. Concentrated virus pellet was dissolved in 100µl PBS overnight at 4°C and aliquoted by 14µl per 1.5ml Eppendorf tube. Aliquoted virus concentrate was frozen in liquid N_2 and stored in -80°C.

The complete process of AOX viral vector production was shown in Fig 7.

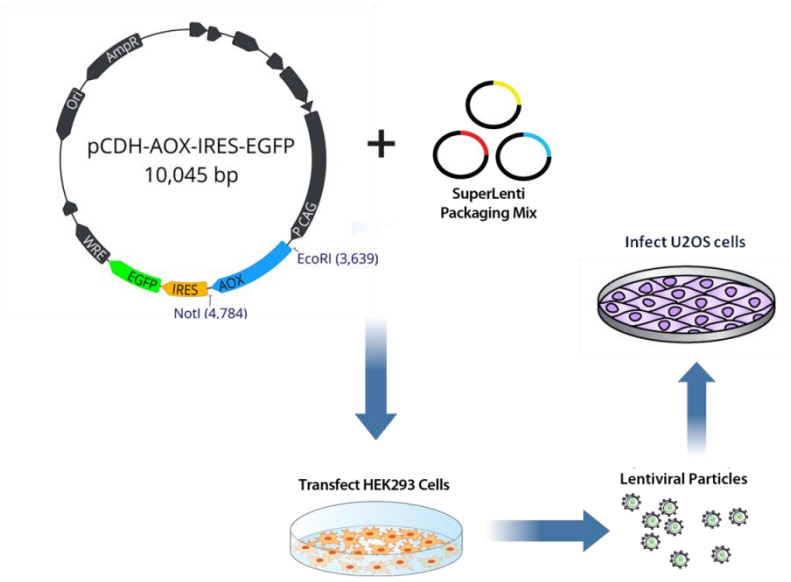

Fig 7. Process of AOX viral vector production and infection

The pCDH-AOX-IRES-EGFP recombinant plasmid was first transfected into HEK293T cells, together with three lentivirus packaging vectors. Then lentiviral particles was integrated and proliferated in the transfected cells. At last the viral particles were collected and concentrated from the cell culture medium and further infected U2OS cells.

2.2.6.5. Viral vector infection

2×10^5 U2OS cells were seeded in each well of 6 well cell culture plate before the day of infection. 14µl of concentrated viral vector and 2µl of polybrene (10mg/ml) were added to medium of cultured U2OS cells (50% confluent). Cells were incubated for 30min at 37^{o}C and spun for 30min at 2500rpm afterwards. Cell culture medium was refreshed after 4 hours. 3 days later, the infection efficiency could be verified with fluorescence microscope.

2.2.7. Immunostaining

2.2.7.1. Antibody immunostaining

U2OS cells were split on the cover slips of the 6 well cell culture plate and cultured in DMEM medium. When confluency reached 50%-70%, cells were washed with PBS and fixed in 4% cold PFA buffer for 15min. Fixed cells were further washed with PBS and permeabilized with 99% cold Methanol for 5min. Permeabilized cells were

washed again with PBS and blocked with 5% BSA-PBST buffer for 1h at RT. Primary antibody was added onto the cover slips for 1h of incubation at RT. Cover slips were washed 3 times and subsequently incubated in diluted secondary antibody for 1h at RT in the dark. After 3 more washes, the cover slips were mounted to glass slides with Vectashield mounting medium and kept at +4^{o}C. Used antibodies are listed below. All the antibodies were diluted in 5% BSA-PBST:

ATP5a (mouse polyclonal) diluted by 1:500
AOX (rabbit polyclonal) diluted by 1:400
Alexa 594 (anti-mouse) diluted by 1:1000
Alexa 568 (anti-rabbit) diluted by 1:1000

2.2.7.2. Nucleic acid staining

1mg/ml of DAPI (4',6-diamidino-2-phenylindole) fluorescence dye was diluted 1:10000 in PBST. Cover slips were incubated in diluted DAPI for 15min in the dark at RT and washed 3 times before mounting.

2.2.7.3. Imaging

All the cover slips were imaged by the fluorescence microscope Imager-M2 (Carl Zeiss) with a high resolution camera (AxioCam HRC), according to manufacturer's instructions. The optimized objective was 40x oil. The contrast reflectors of 38GFP (green), 45TR (red) and 49DAPI (blue) were used. Images were processed with Zen software using same settings. Mitochondrial dynamics was quantified with Image J-win64 software.

2.2.8. Construction of in vitro disease model and AOX rescue test

2.2.8.1. AOX infection on U2OS cell model

On day 1, AOX infection was carried out as described in 2.2.6.5. Cell culture medium

was refreshed on day 2. Infected and uninfected U2OS cells were subcultured 1:3 in a 6 well cell culture plate on day 3.

2.2.8.2. AFG3L2 siRNA double transfection

On day 4, the cell density should be about 50% 7.5µg of AFG3L2 siRNA or scrambled siRNA was pre-mixed with 250µl of Opti-MEM. And 4µl of Lipofectamine RNAiMAX was pre-mixed with 250µl of Opti-MEM. Two parts of solution was combined and mixed gently. After 10min of incubation at RT, 500µl of the mixture was added to the cell culture medium of U2OS cells (WT and AOX infected)

On day 5, siRNA transfected cells were subcultured 1:2 if cell confluency reached 100% and the medium was refreshed. The same process of siRNA transfection was repeated on day 6.

2.2.8.3. Identification of protein expression and mitochondrial fragmentation

On day 7, cell culture medium was refreshed. Cultured U2OS cells were split for immunostaining and western blotting on day 8. For immunostaining, U2OS cells were fixed on day 9 and stained on day 10 according to the protocol 2.2.7. Cover slips were imaged as 2.2.7.3.

For western blotting, U2OS cells were lysed with cell lysis buffer and frozen in -20^{o}C on day 9, followed by protein extraction and western blotting on next day according to the protocol 2.2.3. The entire timing process is depicted as Fig 8.

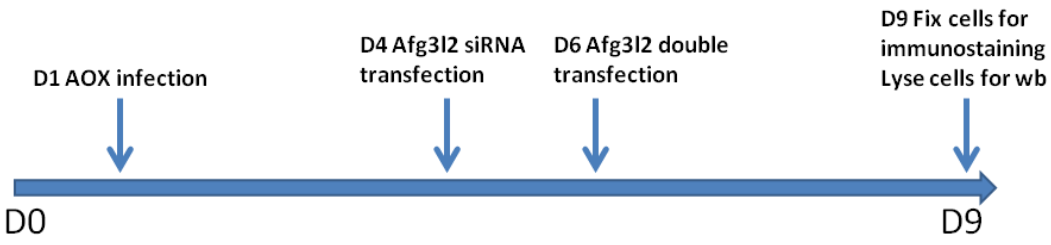

Fig 8. Process of AFG3L2 gene knock down and AOX rescue test on U2OS cell

On day 1 (D1), cultured U2OS cells were infected with AOX lentivirus. On day 4 (D4) and day 6 (D6), infected cells were double-transfected with Afg3l2 siRNA. On day 9, treated cells were collected and divided into two groups. One group of cells was lysed for western blotting (wb), while the other group of cells was fixed for immunostaining.

2.2.9. Statistical analysis

Quantification analysis and calculation of mitochondrial respirometry were performed with Microsoft Excel software. Significance was calculated by student's t-test with GraphPad Prism software. Notable significance was marked as ** ($P<0.005$).

3. Results

The *Rosa26* gene, located on chromosome 6, is an advantageous site for genetic modification in mice. Gene targeting at this site is relatively efficient, and the expression is ubiquitous in many types of cells (Irion et al., 2007). Our transgenic mouse model was created by the insertion of a single *Ciona AOX* gene into the *Rosa26* locus of the mouse embryonic stem cell. After more than 7 generations of backcrossing to strain C57Bl/6J, the transgenic mouse line was maintained stably. The AOX expression of transgenic mice was detected both at mRNA level and protein level by northern blotting and western blotting in all tissues. Uneven expression of AOX was seen in different tissues at both levels, with especially low expression in the brain (Szibor et al., 2017).

3.1. Low expression of AOX in the brain of 1-month-old hemizygous AOX^{Rosa26} transgenic mouse

To verify the preliminary results of low expression level of AOX protein in the brain, repeated western blotting was carried out. Protein samples were extracted from cortex, cerebellum and heart tissue. Genotypes of the protein samples were confirmed by PCR. The western blots in Fig 9 show that AOX protein was expressed much lower in cortex and cerebellum than heart of the 1-month-old hemizygous AOX^{Rosa26} transgenic

mouse. However, SDHA protein seems to be an improper loading control for mice tissue because of unspecific bands (*) shown in cerebellum and cortex.

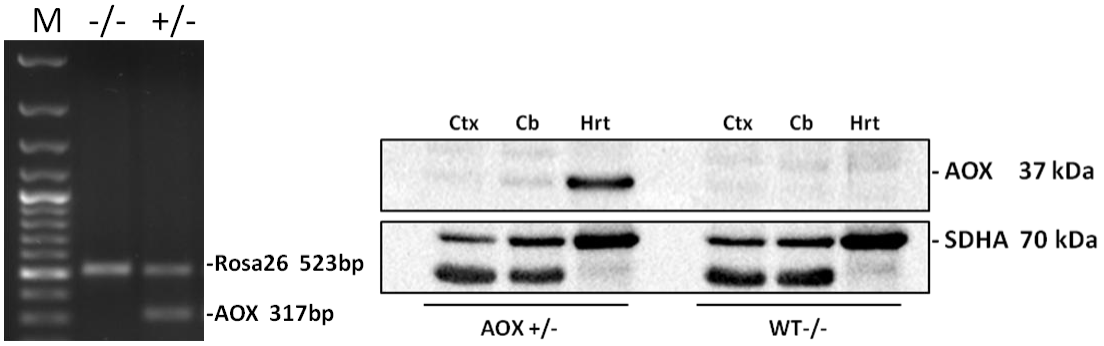

Fig 9. AOX expression in the cortex, cerebellum and heart of 1-month-old hemizygous AOX^{Rosa26} transgenic mice and wild-type mice

(A) Representative PCR results of hemizygous *AOX*^{Rosa26} transgenic mouse and littermate wild-type (WT) control. DNA samples were extracted from the mouse tail snips. The gene ruler is marked as M, and mice genotypes are marked as WT (-/-), AOX (+/-). (B) Western blots of AOX and SDHA proteins from brain and heart. Each sample contains 20μg total protein extracted respectively from cortex (ctx), cerebellum (cb) and heart (hrt) of 1-month-old hemizygous *AOX*^{Rosa26} transgenic mouse and WT control. Blots were probed with antibody AOX 1:50000 and SDHA as loading control. * represents unspecific bands. The result has been confirmed in triplicate.

3.2. AOX expression in the primary neuro-glia cells of new born mice

Neurons are the most important cells in the brain. They undertake the main functions of nerve system, transmitting electrical and chemical signals between each other through synapses, thus regulating metabolism and activity of the whole organism. Neurons are unable to live alone. They need to be supported and protected by glia cells, which help optimize the brain function. Knowing how AOX is expressed in the isolated neuro-glia cells would be meaningful to imply whether it is functional in the brain (Skatchkov et al., 2014; Peng et al., 2014).

Although the expression level of AOX is very low in cortex and cerebellum, this protein can be expressed as high as heart in the primary neuro-glia cells, which were

isolated from the brains of newborn mice (Fig 10). This finding interestingly contradicts the result from Fig 9. To investigate whether the process of neuro-glia cell culture had any effects on the expression of AOX, cultured cells were collected at different time points (1d, 2d, 3d and 4d), and extracted cell proteins were loaded in the same gel to compare the content of AOX protein during the time course of cell culture. By comparing the intensity of target bands between four samples on the western blotting membrane, we could see there was no significant change of AOX expression during the cell culture period.

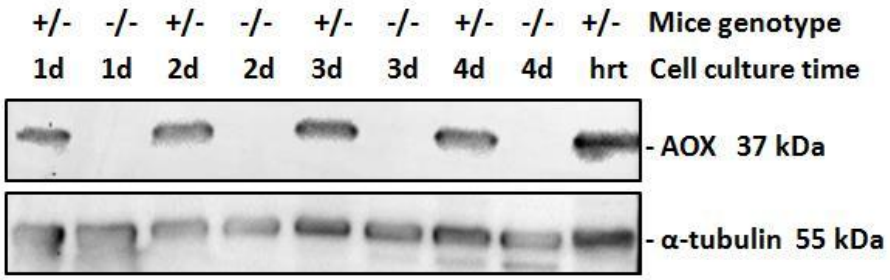

Fig 10. AOX expression in the primary neuro-glia cell of new born hemizygous AOX^{Rosa26} transgenic mice and wild-type mice

Western blots show AOX and α-tubulin proteins of the primary cultured neuro-glia cells from hemizygous *AOX*^{Rosa26} transgenic mice and WT mice born in 3 days. For each sample, 20μg total protein were extracted from the cells, probed with antibody AOX 1:10000 and α-tubulin as loading control. Protein extracted from heart tissue of 1-month-old hemizygous *AOX*^{Rosa26} transgenic mice was loaded as positive control. Cells were collected at different time points during primary cell culture, from 1 day (1d) to 4 days (4d). Genotypes of the cells are marked as AOX heterozygote (+/-) or wild-type (-/-). The result has been confirmed in triplicate.

3.3. Antimycin A resistance of primary neuro-glia cells expressing AOX

Antimycin A is a common toxin for studying cellular responses to the inhibited mitochondrial respiratory chain. This toxin can effectively block the complex III of mitochondrial respiratory chain (Kim et al., 1999) and increase the reactive oxygen species (ROS) in the cells (Maxwell et al., 1999). Excessive antimycin A can even lead to cell death. However, ROS induced by antimycin A decreases significantly in

the presence of AOX, and the damaged respiratory activity is also alleviated in human cells that contain AOX (Matsukawa et al., 2009). To test the functionality of AOX protein in the primary neuro-glia cells, cells expressing AOX and WT cells were treated with antimycin A in DMEM galactose medium for 24h. After the treatment, two cell lines performed different cell viability as shown in Fig 11. Although antimycin A inhibited the cell proliferation comparing treated cells (c,d) with untreated cells (a,b), AOX cells grew better than WT cells under antimycin A treatment. WT cells shrank and detached from the plate while AOX cells remained normal morphology, indicating that WT cells suffered more stress than AOX cells due to the cytotoxicity of antimycin A. Therefore, AOX protein expressed in the neuro-glia cells was functional and could improve the cell resistance to antimycin A.

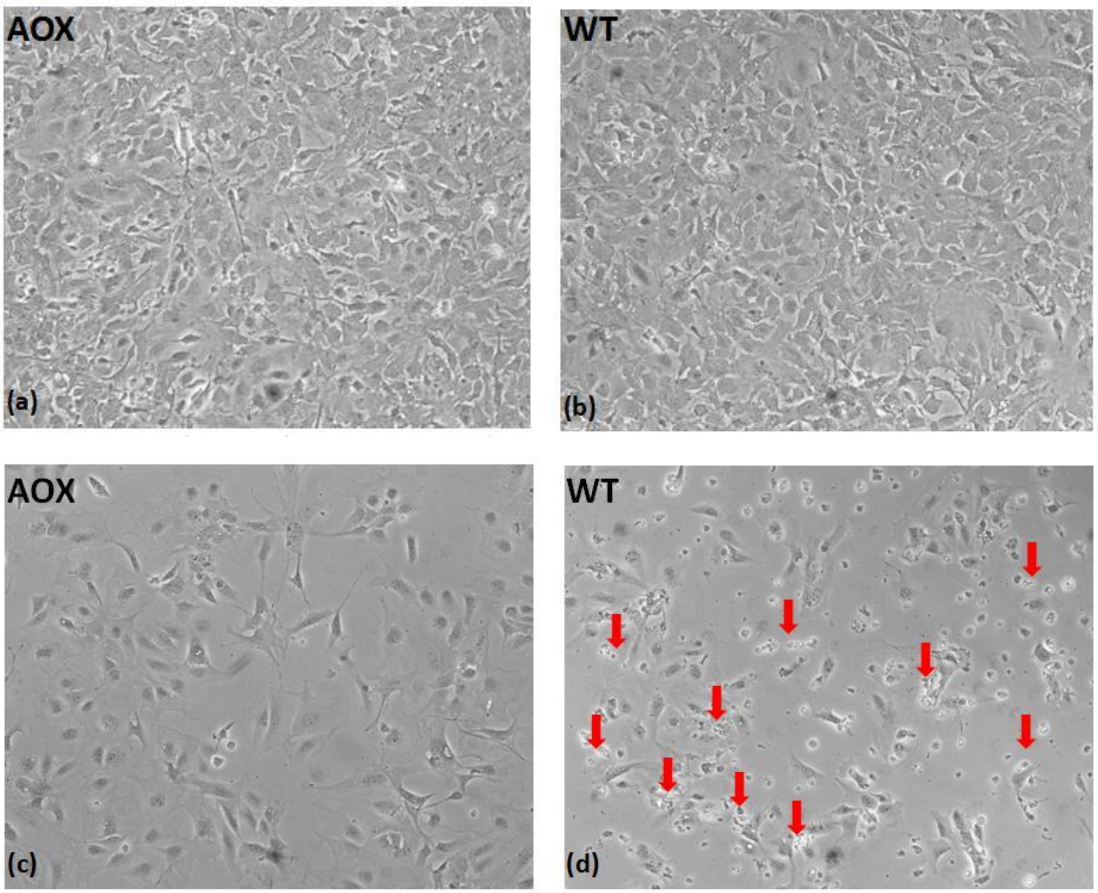

Fig 11. Cell viability of primary neuro-glia cells after antimycin A treatment

Primary neuro-glia cells were isolated from the brains of 3-day-old hemizygous *AOX*^{Rosa26} transgenic mice and WT mice. Cells were cultured in neurobasal A complete medium for 2 days, and transferred to DMEM galactose medium during antimycin A treatment. (a), (b) show the cell

viability of AOX cells and WT cells after 24h culture in DMEM galactose medium. (c), (d) show the cell viability of AOX and WT cells treated with 0.5μM antimycin A for 24h in the same medium. Representative dead cells are pointed out by red arrows. The results have been confirmed in triplicate.

3.4. Buffer optimization for tissue protein extraction

Given the different expression levels of AOX in the brain tissue and neuro-glia cells of transgenic mice, it is easy to associate the inconformity with the possibility that the buffer used for extracting the protein from mouse brain was less efficient compared with those for neuro-glia cells.

To optimize the extraction buffer for AOX protein, three different solutions were tested, including cell lysis buffer (CLB), tissue lysis buffer (TLB) and radioimmunoprecipitation assay buffer (RIPA). Compared with other buffers shown in Fig 12, RIPA buffer demonstrated a slightly better efficiency for protein extraction from the mouse brain. The amount of AOX protein extracted by RIPA buffer was higher than that extracted by cell lysis buffer, which was used for the protein extraction of neuro-glia cells. Therefore, RIPA buffer was selected as the optimized extraction buffer for tissue in the subsequent experiments. Although extraction buffer changed, the expression level of AOX was still much lower in the brain than in the heart, inconsistent with the result of neuro-glia cells.

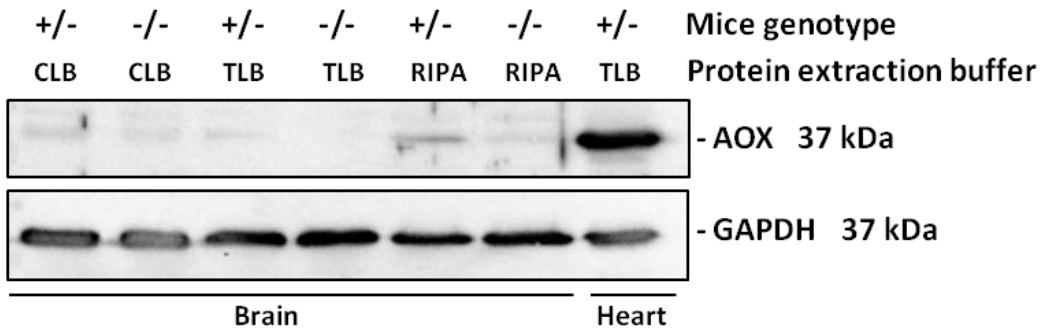

Fig 12. AOX protein extracted from 1-month-old mouse brain by different buffers

Western blots show 20μg total protein extracted from the brain of 1-month-old hemizygous *AOX*^{Rosa26} transgenic mice and WT control, probed with antibody AOX 1:10000 and reprobed for

GAPDH after stripping as loading control. The same brain samples were extracted by cell lysis buffer (CLB), tissue lysis buffer (TLB) and RIPA buffer respectively. Protein from the heart of 1-month-old hemizygous *AOX*^{Rosa26} transgenic mice was used as positive control. Genotypes of the tissue are marked as AOX heterozygote (+/-) or wild-type (-/-).

3.5. AOX expression in the brain of different ages of hemizygous *AOX*^{Rosa26} transgenic mice

Based on the previous findings, the difference of AOX protein level between brain tissue and neuro-glia cells is not due to the efficiency of protein extraction. Another possibility comes out, that the new born mice used for neuro-glia cell culture might have a higher expression level of AOX, than the 1-month-old mice used for tissue extraction in the brain.

To verify this hypothesis and investigate the change of AOX protein in the brain, the hemizygous *AOX*^{Rosa26} transgenic mice brains of four different ages (1 day, 1 week, 2 week, 1 month) were tested and compared with each other. Interestingly, a significant decline of AOX protein level was observed in the brain of hemizygous *AOX*^{Rosa26} transgenic mice along with the increase of age (Fig 13). However, the loading control GAPDH shows uneven level among samples, causing difficulties to compare the amount of AOX protein.

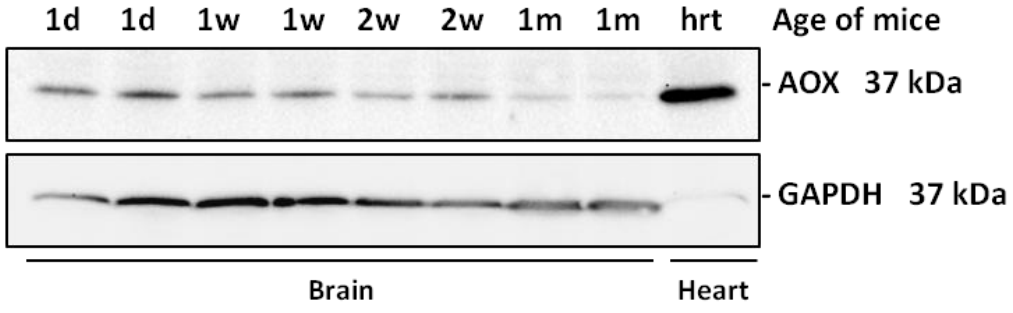

Fig 13. AOX expression in the brain of different ages of hemizygous AOX^{Rosa26} transgenic mice

Western blots show 20μg total protein extracted from the brain of hemizygous *AOX*^{Rosa26} transgenic mice at different ages, probed with AOX antibody 1:10000 and reprobed for GAPDH

after stripping as loading control. Four ages of mice were selected as check point of AOX expression, including 1 day (1d), 1 week (1w), 2 week (2w) and 1 month (1m). Protein from the heart of 1-month-old hemizygous *AOX*^{Rosa26} transgenic mice was used as positive control. Different samples from mice of the same age were loaded in parallel.

3.6. Mitochondrial respiratory activity in the brain and liver of hemizygous *AOX*^{Rosa26} transgenic mice

To test the AOX function in the tissues of hemizygous *AOX*^{Rosa26} transgenic mice, the mitochondrial oxygen consumption rate was measured by oxygraph-2k and recorded by DatLab software. By using different inhibitors and substrates which inhibit or stimulate specific mitochondrial complexes, the respiratory activity of each part of the mitochondrial respiratory chain can be measured according to the oxygen consumption rate (see Fig 14).

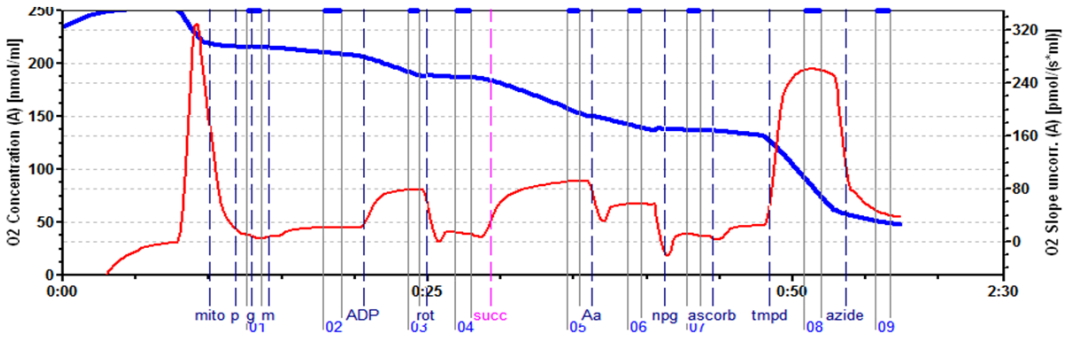

Fig 14. Representative mitochondrial oxygen consumption graph

The change of mitochondrial oxygen consumption activity during 2.5h is shown. Selected values of oxygen slope are marked with numbers from (01) to (09). AOX respiratory activity is correlated with antimycin resistance and can be calculated as the value of [(06)-(07)]/μg protein (mitochondria) per chamber. Complex I activity is calculated as the value of [(03)-(04)]/μg protein (mitochondria). Complex II activity is calculated as the value of [(05)-(07)]/μg protein (mitochondria). Complex IV activity is calculated as the value of [(08)-(09)]/μg protein (mitochondria).

Respiratory activities of three mitochondrial complexes and AOX protein were quantified separately. Respiratory activities of AOX in the brain and liver of different ages (3 day, 4 day, 1 week, 2 week, 4 week) were analyzed and compared side by side. As shown in Fig 15, the decline of AOX respiratory activity in the brain was

correlated with the age, this is also in consonance with the decline of AOX expression. Overall, the AOX respiratory activity in the liver was higher than that in the brain, despite of the fluctuation between different ages. However, the AOX respiratory activity might be underestimated in the liver, because mitochondrial respirometry of liver was always operated later than that of brain due to limited chambers of the oxygraph, meaning that the liver mitochondria were more exhausted than brain mitochondria at the time of measurement. This experiment was only carried out once on account of time limitation, but the result consisted with our expectation.

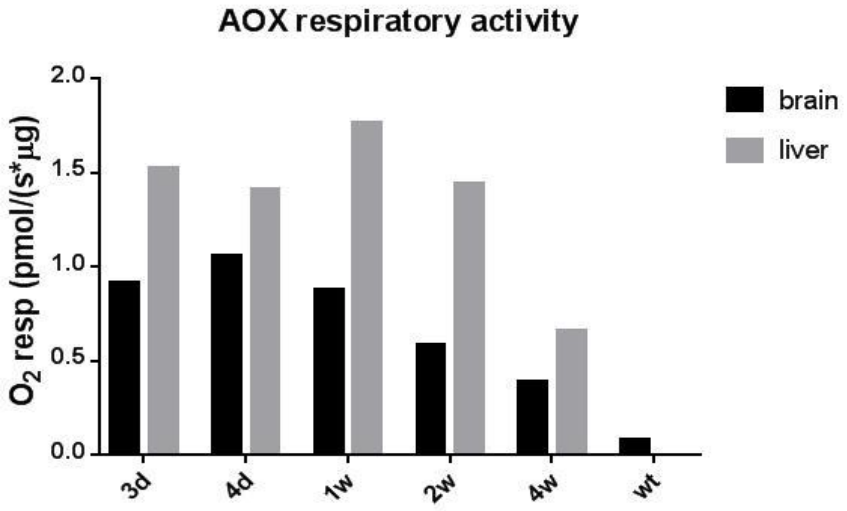

Fig 15. Mitochondrial oxygen consumption activity of AOX in the brain and liver of hemizygous *AOX*^{Rosa26} transgenic mice

Mitochondrial oxygen consumption activity of AOX is shown along with mice age. The mitochondria were extracted from brain and liver of hemizygous *AOX*^{Rosa26} transgenic mice. Mice ages include 3 days old (3d), 4 days old (4d), 1 week old (1w), 2 weeks old (2w) and 4 weeks old (4w). Brain and liver of 3-day-old wild-type mouse (wt) served as negative controls.

In addition, respiratory activities of different mitochondrial complexes were analyzed and compared between the 3-day-old hemizygous *AOX*^{Rosa26} transgenic mice and WT control for both liver and brain, including Complex I, Complex II and Complex IV. As shown in Fig 16, the overall mitochondrial respiratory activity of AOX transgenic mice was higher than WT mice, and that of brain was higher than liver. Only complex II was an exception. However, more data should be collected to analyze the significance of difference before drawing a conclusion, because we only carried out

the experiment twice for AOX transgenic mice and once for WT mice due to limited materials.

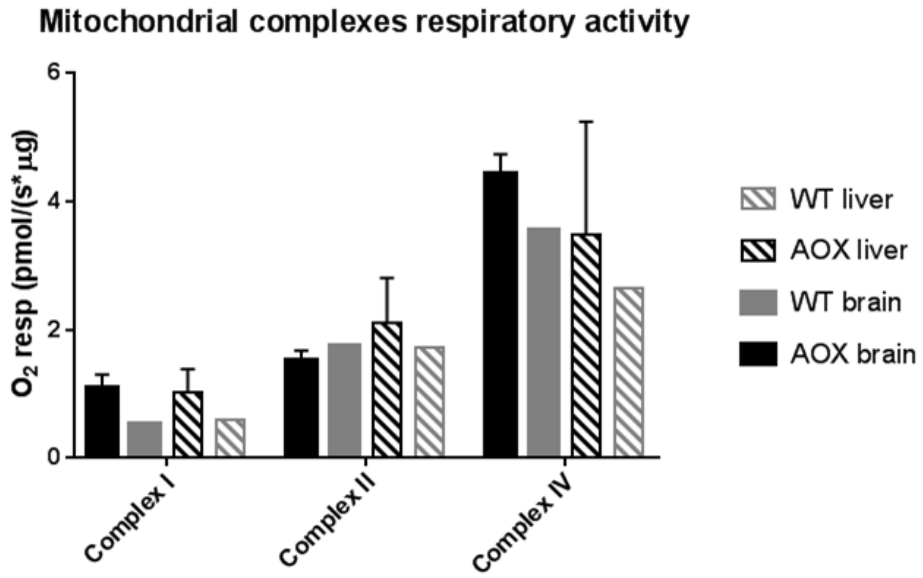

Fig 16. Oxygen respiratory activity of three mitochondrial complexes in the brain and liver of hemizygous *AOX*^{Rosa26} transgenic mice

Mitochondrial respiratory activities of Complex I, Complex II and Complex IV were measured by oxygraph-2k and graphed by GraphPad Prism. The mitochondria were extracted from brain and liver of 3-day-old hemizygous *AOX*^{Rosa26} transgenic mice and WT mice at the same age. Error bars represent means±SD of two independent experiments.

3.7. AOX viral vector construction and infection on U2OS cells

In order to study the AOX function in the adult mouse brain and human cells, a lentiviral vector was constructed to induce the expression of AOX. The DNA plasmid that drove the expression of AOX was designed as Fig 6, with *Ciona intestinalis AOX* gene, the synthetic promoter (*pCAG*), the antibiotic marker of ampicillin (*AmpR*), the internal ribosome entry site (*IRES*), the enhanced green fluorescent protein gene (*EGFP*), the Woodchuck hepatitis virus Post-transcriptional Regulatory Element (*WRE*) and the restriction sites *EcoRI* and *NotI*. The function of *pCAG* and *WRE* is to initiate and enhance the expression of *AOX* and *EGFP* gene. Sizes of both the insert

gene segment and plasmid backbone were verified by restriction digest and agarose electrophoresis (see Fig 17 A). The lentiviral vector was integrated by the *AOX* plasmid and three packaging plasmids, including pRRE, pRSV and pMD2.G. Integral lentivirus was further proliferated in HEK293T cells and concentrated by ultracentrifugation. Thus, the AOX gene could be delivered into the genome of U2OS cell through virus infection. The expression of AOX in these cells was confirmed by both western blotting (see Fig 17 B) and immunostaining (see Fig 18). The infection efficiency was about 30%.

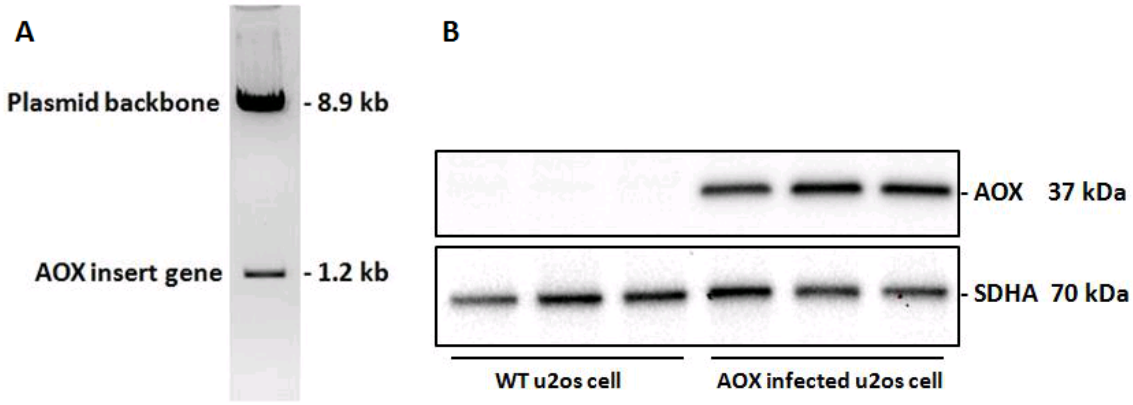

Fig 17. AOX plasmid digestion and AOX viral vector infection on U2OS cells

(A) The constructed AOX plasmid digested by restriction enzymes EcoRI and NotI. DNA fragments are shown on the agarose gel. The genes and sizes of two DNA fragments are annotated beside the bands. (B) Western blots of 15μg total protein of the AOX lentivirus infected cells and WT cells. Blots were probed with antibody AOX 1:10000 and SDHA as loading control.

Along with *AOX*, the *EGFP* gene was also expressed in the infected U2OS cells (see Fig 18 A). The purpose of inserting this gene into the plasmid is to track AOX by the enhanced green fluorescence protein. Interestingly, the expression levels of AOX and EGFP were not completely matched in the infected U2OS cells. In some cells, the green fluorescence from EGFP was invisible while the red fluorescence provided by AOX antibody was clear (see Fig 18 B). And the intensity of green fluorescence varied from cell to cell. This phenomenon indicated that the expression of EGFP was not be as stable as AOX in the infected U2OS cells, which might result from the regulation of *IRES* gene.

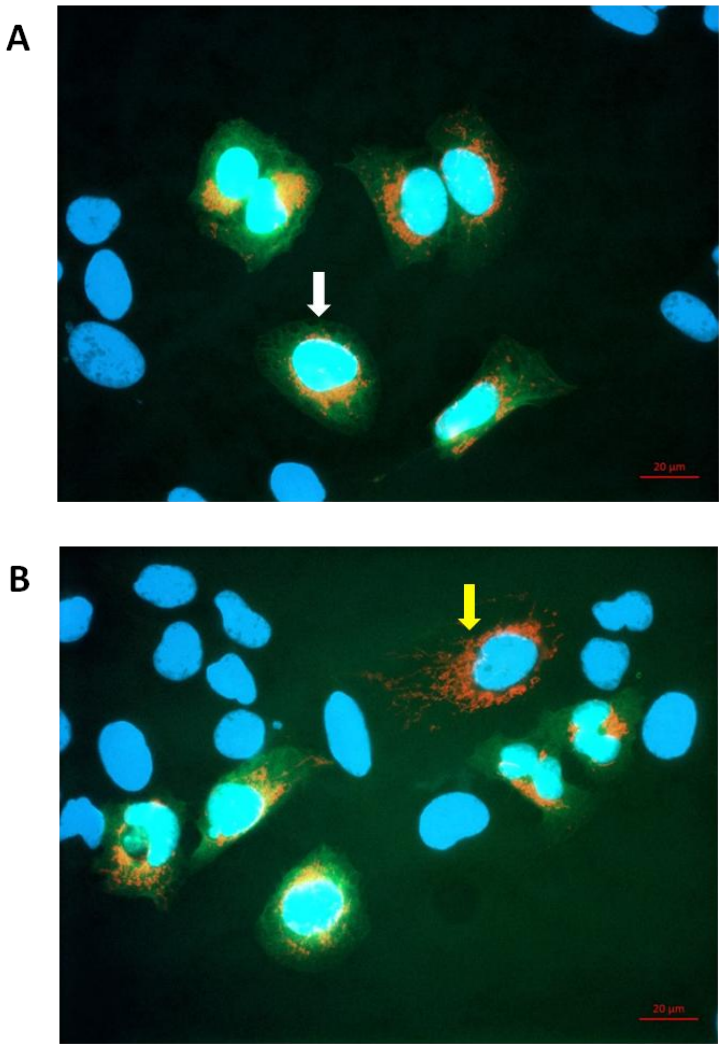

Fig 18. Representative immunostaining image of AOX infected U2OS cells

The U2OS cells infected by AOX lentivirus were stained by AOX antibody in the mitochondrial membrane (*red*) and DAPI in the nucleus (*blue*). The enhanced green fluorescence protein (EGFP) was expressed in the infected cells (*green*). Scale bar 20µm. (A) Colocalization of EGFP and AOX in infected U2OS cell (*white* arrow). (B) Non-colocalization of EGFP and AOX in infected U2OS cell (*yellow* arrow)

3.8. *AFG3L2* gene knock down in vitro model and AOX lentivirus rescue

We constructed the lentiviral vector in order to express the *AOX* gene in different cell lines or animal models, so that the function of AOX protein could be tested under certain conditions. Our interest is to investigate whether AOX has an effect on neurodegenerative diseases. Many neurodegenerative diseases are associated with

defects in mitochondrial respiration and mitochondrial dynamics. SCA28, caused by haploinsufficiency of *AFG3L2*, shows mitochondrial features such as respiratory deficiency (Di Bella et al., 2010), mitochondrial fragmentation (Karbowski and Neutzner, 2012) and ineffective mitochondrial Ca^{2+} handling (Maltecca et al., 2015). Therefore, we built an in vitro disease model by knocking down the *AFG3L2* gene in U2OS cells to mimic the neurodegenerative disease condition of SCA28. The *AFG3L2* gene was transiently silenced in the U2OS cells by siRNA double transfection. By comparing the target characteristics of wild-type cells and AOX lentivirus infected cells, before and after the AFG3L2 siRNA transfection, we could evaluate the AOX potential of treating the disease.

The infection of AOX lentivirus was accomplished three days before the *AFG3L2* gene knock down, ensuring that the U2OS cells expressed AOX and EGFP at the time of siRNA transfection. As a result of siRNA interference, the expression of AFG3L2 protein decreased dramatically, both in the WT cells and AOX cells (see Fig 19).

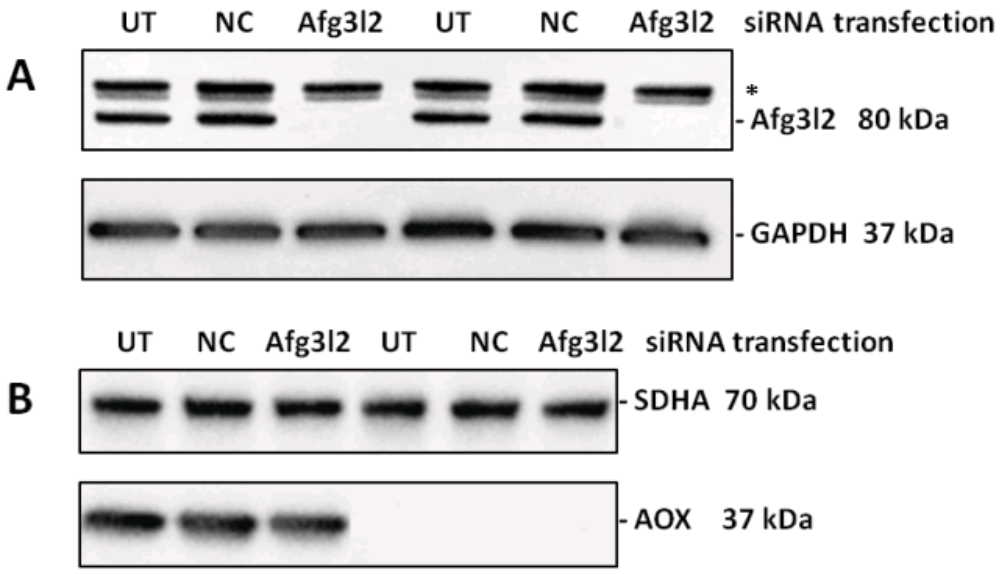

Fig 19. Protein expression of AFG3L2 and AOX in the U2OS cell disease model

Western blots show different proteins in AOX lentivirus infected U2OS cells and wild-type control, 3 days after double-transfection with AFG3L2 siRNA (Afg3l2) or scrambled siRNA (NC). (A) 10μg of total protein samples probed with AFG3L2 antibody and reprobed for GAPDH. (B) 15μg of the same protein samples probed with AOX 1:10000 and reprobed for SDHA. Untransfected cells (UT) served as negative control. * represents unspecific bands. The results have been

confirmed in triplicate.

OPA1 is one of the important proteins that regulates mitochondrial quality control. This protein has different isoforms in different organisms. Knocking down of *AFG3L2* causes the destabilization of OPA1 protein, especially for the long isoform (L-OPA1) (Ishihara et al., 2006; Ehses et al., 2009). Therefore, western blots show different protein patterns of OPA1 after the AFG3L2 siRNA transfection (see Fig 20). The L-OPA1 degraded along with the silencing of *AFG3L2* in U2OS cells, which was a sign of mitochondrial abnormality. The OPA1 patterns in AOX infected cells seemed the same as in WT cells, indicating that AOX protein failed to rescue the cleavage of L-OPA1 in the AFG3L2 defective U2OS cells. However, this result is not sufficient to demonstrate the relationship between AOX and OPA1. Many factors should be considered to judge the impact of AOX on these excessively manipulated cells.

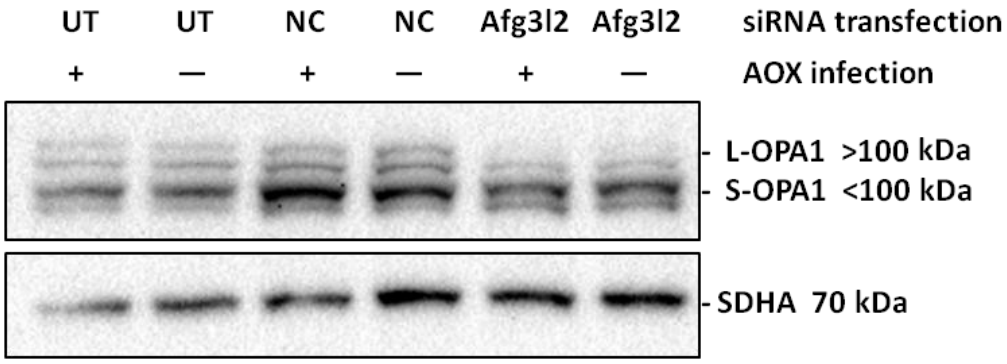

Fig 20. OPA1 expression in the U2OS cell disease model

Western blots show 10μg total protein of WT and AOX lentivirus infected U2OS cells, after double-transfection with AFG3L2 siRNA or scrambled siRNA (NC). Blots were probed with OPA1 antibody and reprobed for SDHA as loading control. The OPA1 protein was present as two types of isoforms (L-OPA1 and S-OPA1) under normal condition, whereas the L-OPA1 disappeared after knock down of *AFG3L2* gene. Untransfected cells (UT) served as the negative cell control, while NC served as the negative transfection control.

AFG3L2 is an important protease that regulates the process of OPA1 cleavage (Ehses et al., 2009). Loss of AFG3L2 can induce many cellular responses (Maltecca et al., 2012; Kondadi et al., 2014), here we only focused on the changes of mitochondrial morphology in the cell. Therefore, we immunostained the U2OS cells after AFG3L2 siRNA transfection and observed the mitochondria morphology in these cells. Mainly two types of mitochondrial structures were found: tubular and fragmented

mitochondria (see Fig 21 A). To quantify the difference of mitochondria morphology between AOX and WT cells, we scored the number of cells that contained tubular and fragmented mitochondria separately (see Fig 21 B). As expected, the cell number of tubular mitochondria decreased, while that of fragmented mitochondria increased significantly in the *AFG3L2* knock down cells compared with the scrambled siRNA transfected cells. There was no significant difference of mitochondrial morphology between AOX and WT cells after scrambled siRNA transfection. Interestingly, AOX cells showed significantly less fragmented mitochondria than WT cells after the AFG3L2 siRNA transfection. This difference indicates that AOX might alleviate the disadvantages caused by loss of AFG3L2 and retain the normal mitochondrial morphology independently of OPA1 cleavage.

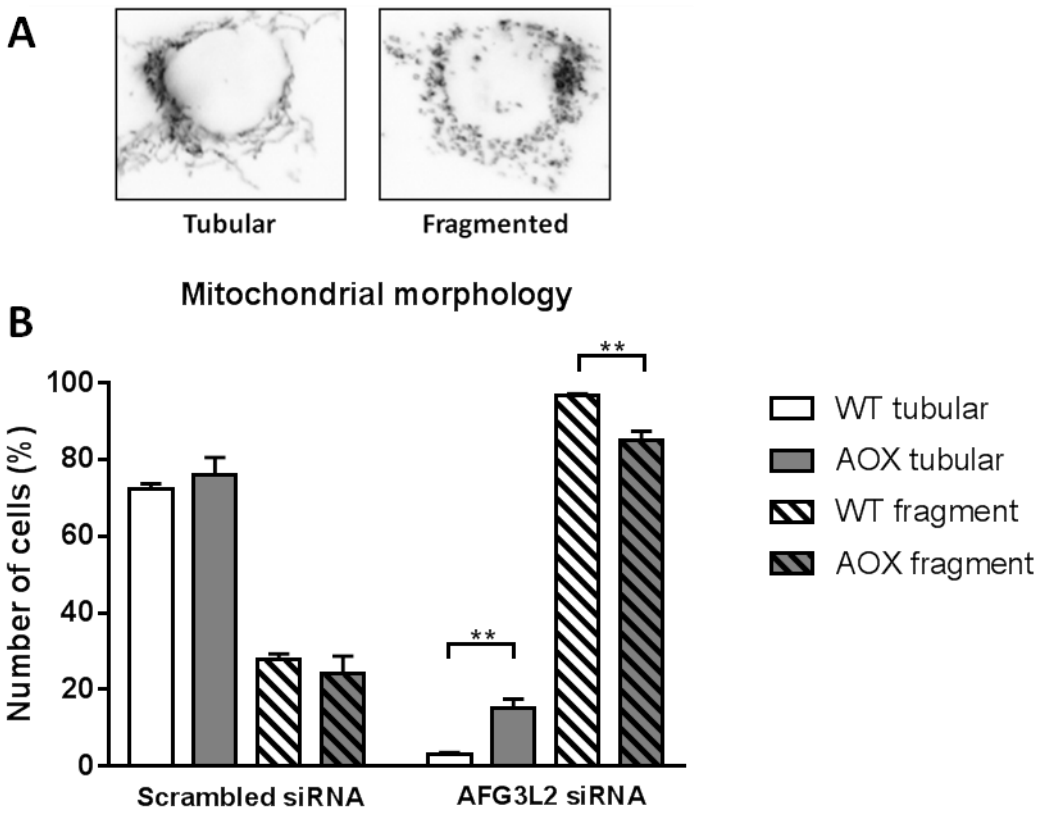

Fig 21. Mitochondrial morphology in the U2OS cell disease model

(A) Representative images of U2OS cells with tubular and fragmented mitochondria. Mitochondria were immunostained with ATP5a antibody. (B) Quantification of mitochondrial morphology in U2OS cells, transfected with scrambled siRNA or AFG3L2 siRNA, wild-type cells (WT) or AOX lentivirus infected cells. Tubular and fragmented mitochondria were scored and calculated as number of cells (%). Error bars represent means±SD of three independent experiments; ** represents $P < 0.005$ by Student's t test. Sample sizes for scrambled siRNA are as

follows: n=96, n=129, n=116 cells counted for WT cells in each independent experiment respectively; n=55, n=13, n=25 cells counted for AOX cells. Sample sizes for AFG3L2 siRNA: n= 122, n=174, n=150 cells counted for WT cells respectively; n=71, n=25, n=41 cells counted for AOX cells.

4. Discussion

4.1. AOX expression and activity in the transgenic mouse brain

Low expression of AOX was observed in the cortex and cerebellum of adult transgenic mice. We confirmed this result by repeated western blotting with samples from different individuals and different concentrations of AOX antibody (1:50000 and 1:10000). Protein sample from the heart was used as positive control because AOX was expressed at high level in the heart. However, it was still unknown whether the low expression level of AOX in the brain should be functional or in vain at this point. According to related studies on yeasts and fungi (Veiga et al., 2000; Nargang et al., 2012), AOX shows barely activity under normal conditions but can increase its expression and become active when the mitochondrial respiratory chain is disturbed.

The regulation of AOX is highly complex in different species and the activity of AOX is determined by various factors. The expression of AOX can be induced or inhibited in different conditions of organisms, tissues and cell types (Rogov et al., 2014). Thus, we isolated neuro-glia cells from the transgenic mouse brain to further study the expression and activity of AOX at cell level, as this cell type is especially important for neurodegenerative diseases. Surprisingly, the amount of AOX protein in the cultured neuro-glia cells was as high as that in heart tissue of 1-month-old transgenic mice. Besides, the antimycin A treatment test on the neuro-glia cells indicated that AOX protected the transgenic cells against the toxin and improved cell survival compared with WT cells. Although this result might not be convincing enough to identify specific function of AOX in neuro-glia cells, since cell apoptosis is a complex process affected by many other factors. At least the increased cell survival rate reflected the activity of AOX and assured that this protein is functional. Similar

results acquired from other cell lines have also given implications for the feature of AOX in neuro-glia cells (Hakkaart et al., 2006; Matsukawa et al., 2009), suggesting that antimycin A resistance can be considered as a reference indicator for the AOX activity. More quantifications should be done to verify the result as well as elaborating the functions of AOX, such as reduction of cellular ROS and oxygen consumption ability. However, the limited lifetime and rigid culture condition of primary neuro-glia cells restricted the application of many measurements.

Based on the different expression level of AOX in the brain tissue and neuro-glia cells, several assumptions were proposed to explain this result. The first assumption was that, the expression of AOX could be induced during the cell culture process. AOX expression and activity are associated with the availability of nutrients and environmental conditions on the basis of posttranslational regulation. Neuro-glia cells cultured in vitro encounter high concentration of oxygen, abundant substrates and specific growth factors in the medium, which are highly different from the conditions in vivo. As a result, the expression of AOX might be up-regulated in the neuro-glia cells compared with that in the brain. In order to prove this assumption, we cultured the primary neuro-glia cells for four days, collecting cell samples every day, from the first day when cells were isolated, to the last day that cells could survive. However, no significant difference was found between the AOX contents of neuro-glia cells collected from each day, which meant the cell culture condition was not the reason of maintaining high expression level of AOX in the neuro-glia cells.

The second assumption then arose, the protein extraction efficiency of AOX was not as high in the brain tissue as in the heart tissue and cells. This assumption was based on the special characteristics of AOX protein and brain. On one hand, AOX is an integral membrane protein which can be found in the mitochondrial membrane (Berthold and Stenmark, 2003). The structure of AOX contains a hydrophobic region tightly associated with the phospholipid head group, requiring detergent to separate this protein from the membrane (Berthold et al., 2000). Thus, the AOX protein is not as easily extractable as water-soluble proteins, and it is even harder to be solubilized and purified from animals than plants (Chaudhuri et al., 1995). On the other hand, brain is a special organ that contains large proportion of fat, which triggers more difficulties to the extraction of AOX protein. We compared the protein extracted in the

tissue lysis buffer with protein left in the cell pellet by western blotting. The level of AOX protein was surprisingly higher in the pellet than in the buffer (data not shown). Therefore, we tested three buffers to compare their extraction efficiency, including the cell lysis buffer used for the neuro-glia cells, the tissue lysis buffer used for the brain and heart tissues, and the RIPA buffer which is widely used for protein extraction. Although the RIPA buffer slightly increased the extraction efficiency of AOX protein, the expression level of AOX was still very low in the brain tissue compared with heart and neuro-glia cells. In addition, we also tested different extraction methods but none of them improved the amount of AOX protein extracted from the brain tissue.

The third assumption was finally proved to be true, which suggested that the expression level of AOX in the brain was changed along with the age of transgenic mice. It has been reported that AOX expression can be various at different developmental stages in some organisms, such as *Trypanosoma brucei* (Walker et al., 2005), *Yarrowia lipolytica* (Guerrero-Castillo et al., 2012) and *Metarhizium anisopliae* (Uribe et al., 2008). The mice used for neuro-glia cell isolation were newborns at the age of 1-3 days old, while the age of the mice used for brain tissue extraction was over 1 month. Thus we had good reason to suspect that the AOX expression in the brain was different between these mice. In fact, a decline of AOX expression was clearly detected in the brain from the 1-day-old pups to the 1-month-old mice according to our result. On account that the antibody SDHA bound unspecific protein in the brain tissue, GAPDH was used to replace it as loading control. However, GAPDH also demonstrated limitations. The difference of GAPDH level between protein samples was probably resulted from the stripping process. Because GAPDH has a similar size to AOX, stripping is necessary for removing the AOX antibodies bound to the membrane and reprobing the samples with GAPDH antibodies. During the process of stripping, loss of protein was unavoidable, which might lead to reduced intensity of bands during chemiluminescent detection. To eliminate the effect of stripping, same samples should be ran in two gels in parallel, so that each membrane could be probed by different antibody at the same time. Moreover, although GAPDH is relatively stable across species as a housekeeping protein, the expression of this protein varies among different tissues (Barber et al., 2005; Ferguson et al., 2005). Hence, the loading control bands of heart and brain in Fig 13 were not even, suggesting that GAPDH was not an appropriate reference protein for both brain and heart tissue in this case.

The expression level of AOX in the transgenic mouse brain was associated with the AOX activity, which also decreased along with the age (from 4-day-old to 4-week-old). Although there was a slight increase from 3 to 4 days old, more data should be collected to find the peak. Here, the AOX activity referred to the oxygen consumption ability of mitochondria or mitochondrial respiratory activity through the alternative pathway provided by AOX. This activity was measured by OROBOROS oxygraph-2k, a widely used respirometer in mitochondrial research (Aidet et al., 2013; Kim et al., 2015; Patel et al., 2015). Mitochondria isolated from the liver were used as the positive reference as AOX was highly expressed in this organ. Compared with liver, the AOX activity in the brain was always lower. Furthermore, the activities of other complexes in the mitochondrial respiratory chain were also measured for 3-day-old mice, suggesting that the hemizygous AOX^{Rosa26} transgenic mice had higher complex activities than the WT mice, and the activities were higher in the brain than in the liver except for complex II. According to these findings, we suggest that AOX could improve the level of mitochondrial respiration. But the activity of AOX was lower in the brain compared with liver due to higher activities of other mitochondrial complexes in the brain. This is in accordance with the balancing characteristic of AOX whose activity can be induced by inhibition of main respiratory pathway while alternatively reduced in response to high respiration through the main pathway. However, lacking of repetitive experiments drew these results back before making solid conclusions. In addition, the complicated procedure of the mitochondrial isolation and limited chambers of oxygraph-2k respirometer caused mitochondria of the liver less healthy than those of the brain, leading to inaccuracy of the comparison between two tissues.

To sum up, the most important result indicates that the expression and activity of AOX protein in the brain decreased substantially within one month. On the basis that preliminary results also showed a low mRNA level of AOX in the adult mouse brain (data not shown), the expression of *AOX* gene might have already been down-regulated since transcription. The regulatory mechanism in the brain was so

complicated that we could not determine which pathway was the leading factor. But at least these results provided a prediction that AOX protein might not show significant function in the brain of an adult hemizygous *AOX*^{Rosa26} transgenic mouse. Therefore, if we still insisted to study the function of AOX protein in the brain, we had to establish a biological tool to induce its expression.

4.2. Lentiviral vector construction and AOX expression in virus infected cells

Virus is a useful biological tool for introducing foreign protein in vivo or in vitro because of its infection ability. Compared with the DNA plasmid transfection, virus infection is less toxic to the cells and the time of gene expression is more flexible based on virus types. Among all the viral vectors, lentivirus has its unique advantage of integrating the transgene into the host genome so that the target protein can be expressed in the daughter cells. The 3rd generation lentivirus packaging system has made the application of lentivirus safer than before as the viruses integrated in the cells are unable to proliferate by themselves. Therefore, we chose lentivirus to construct the viral vector for stably expressing *AOX* gene in mammalian cells. However, lentivirus infection also has disadvantages. The copy number of the target gene and the insertion site on the host genome are uncontrollable after infection. Different copy numbers causes that the expression level of target gene varies from cell to cell. And incorrect gene insertion can even lead to cell death.

The U2OS cell line is a fast growing cancer cell line isolated from the human osteosarcoma. Mitochondrial morphology is maintained well in this cell line and clearly observed after immunostaining under microscope. Moreover, the MOI (multiplicity of infection) value for lentivirus and U2OS cell is low, which means U2OS cell can be easily infected by lentivirus. Thus we used the constructed AOX lentiviral vector to infect U2OS cell line for studying the AOX function in the mitochondria. According to the immunostaining result, only 30% of the cells showed

the presence of AOX protein, whereas the western blotting result showed high level of AOX compared with the reference protein SDHA, indicating that AOX could be over-expressed in the infected cells. As one of the mitochondrial membrane protein, the distribution of AOX reflected the morphology of mitochondria.

The low efficiency of virus infection might depend on many factors. Since virus invading is harmful to the cell, the non-infected cells gain advantages of cell growth and generally take up the majority of cell population. The exogenous gene would inhibit cell division or stimulate cell apoptosis if they were inserted into critical locus of the host genome. Additionally, the exogenous gene itself can be disadvantageous to the cell. Unfortunately, the AOX lentiviral vector contained no selective marker for screening infected cells. Therefore, we could not isolate positive clones and specifically amplify them in selective medium.

In addition to *AOX*, the *EGFP* gene was also expressed by the lentiviral vector in U2OS cells. The green fluorescence protein (GFP) encoded by *EGFP* is a popular marker to track the expression of target gene as the GFP is easily observed under fluorescent microscope. Since AOX protein was only visualized after binding to the fluorescent antibody, GFP could preliminarily indicate whether the gene cassette carried by lentivirus was successfully integrated into the cell. Theoretically, the *AOX* and *EGFP* genes should be expressed at the same level in each cell. However, the immunostaining images demonstrated the opposite result, revealing that the expression level of *EGFP* was quite uneven in the U2OS cell population compared with *AOX*. The reason might lie in the *IRES* site that connected *AOX* and *EGFP* gene in the plasmid cassette. The *IRES* site is the RNA sequence that allows the ribosome to bind the internal sequence and initiate the translation via a cap-independent mechanism (Pelletier and Sonenberg, 1988). With this site, co-expression of two independent genes can be driven by a single promoter. However, the second gene translated by IRES site has been reported to have lower expression than the first gene in a bicistronic vector (Mizuguchi et al., 2000). This difference should have been

considered before constructing the vector, as long as we expected the same expression level of reporter gene and target gene. Although the expression of GFP was unstable in the infected cells, a cell containing GFP should express AOX as well. A flow cytometer could be used to select AOX positive cells based on fluorescent signals. But due to limitation of time and equipment, we gave up positive cell isolation.

4.3. AOX function and application in the neurodegenerative disease model in vitro

Some traditional functions of AOX have already been verified in the brain tissue and neuro-glia cells of newborn transgenic mice, including the antimycin A resistance and oxygen consumption ability in mitochondria. But how does AOX function under disease condition? Can AOX alleviate symptoms triggered by mitochondrial defects? Since the expression of AOX in the adult mice is low, will it be induced by the stress of diseases? These are the main questions in regard to the feasibility of AOX application in neurodegenerative diseases. And the purpose of lentiviral vector construction is to answer the questions by introducing AOX into disease models.

We established an in vitro disease model to mimic the SCA28 disease. SCA28 is a representative neurodegenerative disease that shows defects of mitochondrial respiratory chain and fragmentation of mitochondrial network. This disease is caused by mutations in the *AFG3L2* gene that encodes a mitochondrial protease (Di Bella et al., 2010). It is known that AOX can compensate the blocked mitochondrial respiratory chain and reduce ROS production, but whether it can regulate or interact with mitochondrial quality control proteins such as AFG3L2 has not been proved. To test the AOX function in this in vitro disease model, we first infected U2OS cells with AOX lentivirus. When the GFP signal was observed in the cells, we knocked down the *AFG3L2* gene of these cells by siRNA double transfection. No band of AFG3L2 protein was detected on western blots after the double transfection. As *AFG3L2* gene regulates the processing of OPA1, an important protein for mitochondrial fusion,

AFG3L2 gene silencing can cause L-OPA1 cleavage and mitochondrial fragmentation. Therefore, we evaluated the AOX function by comparing these two results in WT cells and AOX lentivirus infected cells before and after *AFG3L2* silencing. To eliminate the impact of transfection on the cells, the samples also included cells transfected with scrambled siRNA as negative control. But no difference was found between untreated cells and the negative control.

OPA1 is not only responsible for mitochondrial fusion, it also interacts with complex I, II and III of the mitochondrial respiratory chain, stimulates electron transportation and prevents proton leakage (Duvezincaubet et al., 2006; Lenaers et al., 2009). In addition, OPA1 can resist cell apoptosis via cristae remodeling (Olichon et al., 2003; Cipolat et al., 2006) Based on the western blot of OPA1, L-OPA1 was lost after *AFG3L2* gene knock down, both in WT cells and AOX cells. The complete transition of L-OPA1 to S-OPA1 might result from inhibition of mitochondrial respiration or induction of cell apoptosis. Although AOX seems not to prevent the degradation of L-OPA1, several reasons can explain this result. First, compared with various stresses that the cells suffered from both the process of virus infection and siRNA transfection, the effect brought by AOX might be too small to alleviate the OPA1 destabilization caused by these stresses as well as AFG3L2 knock down. Second, the impact of AOX might not be as significant as AFG3L2 on the regulation of OPA1 processing. More extremely, AOX might not even play a role in rescuing OPA1 degradation at all. Therefore, AOX failed to maintain the normal pattern of OPA1 after *AFG3L2* silencing. Despite of all the possible reasons, a conclusion was still too early to be drawn unless more repeated experiments were carried out to verify this result. Even though AOX can not prevent OPA1 destabilization, it may still rescue the defective cells from other aspects.

Abnormal mitochondrial morphology has been commonly found in neurodegenerative diseases (Knott and Bossy-Wetzel, 2008; Chen and Chan, 2009; Su et al., 2010). Mitochondria in the respiratory active cells normally form a fusion network to exchange metabolites and mtDNA, whereas in resting or damaged cells mitochondria

are represented as fragmented structures (Westermann, 2012). It has been reported that mitochondrial fragmentation caused by dysfunction of mitochondrial protein synthesis, is a key reason for AFG3L2-related neurodegeneration (Almajan et al., 2012). Therefore, it would be interesting to see whether AOX could protect the mitochondria in the disease model by recovering the balance of mitochondrial dynamics. In normal condition, mitochondria were fused with each other and together constructed a tubular network. However, when *AFG3L2* gene was knocked down, this network was disrupted and lead to fragmented mitochondria. According to our statistical result, less fragmented mitochondria were shown in the cells infected by AOX lentivirus than WT cells after AFG3L2 siRNA transfection, which suggested that AOX might be beneficial to balance the mitochondrial dynamics. This is a very interesting finding. As discussed previously, the OPA1 cleavage pattern was not changed in the presence of AOX, meaning that AOX might not rescue the OPA1 destabilization caused by AFG3L2 defects. However, the most significant result brought by OPA1 degradation—the mitochondrial fragmentation—was alleviated by AOX regardless of OPA1 rescue, contradicting to the common belief that OPA1 cleavage is the essential reason for mitochondrial fragmentation based on AFG3L2 dysfunction. According to revealed functions of AOX, this alleviation may due to reduced oxidative stress, compensated electron transport chain, improved metabolic and signaling homeostasis (Vanlerberghe, 2013), or decreased susceptibility to programmed cell death (Li and Xing, 2010). More boldly assuming, AOX might even affect other mitochondrial fusion or fission proteins through unknown mechanisms or regulate pathways that are important for protecting the mitochondrial network. Among all the potential elements, the relationship between mitochondrial respiration and mitochondrial membrane dynamics is of great significance to explore, as AOX is especially active for maintaining mitochondrial respiratory chain. The significant reasons leading to mitochondrial fragmentation besides OPA1 cleavage probably include respiratory defects. Although it is hard to determine which factor brought by AOX mainly prevents the mitochondrial fragmentation without further identification, this result indicates a new perspective for studying mitochondrial dynamics and for

seeking potential therapy to treat mitochondrial diseases.

To be more objective, many conditions should be considered to evaluate the reliability of this result. First, the sample size of AOX cells was much smaller than WT cells. Because the infection efficiency of AOX lentivirus varied between different batches of cells and was relatively low overall. Difficulties arose when looking for positive cells with EGFP fluorescence. Second, the resolution of images was not ideal with the fluorescence microscope, further decreasing the number of cells with distinguishable mitochondrial morphology. Third, the manual scoring method might lead to bias for classifying different mitochondrial morphology, since many cells were neither completely tubular nor fragmented but looked like a shape in between. Fourth, both processes of virus infection and siRNA transfection triggered stress to the cells. Thus, the effect of AOX might not only target at rescuing the defects caused by loss of AFG3L2 but might also alleviate other cell damages during the process. Fifth, although the western blot showed that AFG3L2 protein were absent in the transfected cells overall, we could not confirm AFG3L2 was knocked down in every single cell selected for quantifying the mitochondrial fragmentation, which might cause controversial result of the quantification. Unfortunately, the whole process of this experiment took more than 10 days, hence we have no time to repeat it more times and collect more data.

Considering all the drawbacks, there are definitely improvements that we can make for the future experiments. Most importantly, a selective marker in the viral vector is necessary for the cell screening as the infection efficiency is relatively low. If we could selectively clone the positive cells which expressed AOX, the time of establishing the *AFG3L2* knock down cell model would be shorter and cells could recover from the virus infection before transfection. Secondly, since siRNA transfection can only silence the *AFG3L2* gene transiently, the shRNA transfection may be used to knock down the target gene for longer time and is better for further functional analysis. Thirdly, the quantification method of mitochondrial morphology

should avoid bias. Some innovative quantitative analysis of mitochondrial morphology have been developed to replace simple manual quantification, including high-content imaging based on machine learning (Leonard et al., 2015), super-resolution imaging coupled with membrane potential analysis (Jakob et al., 2015), and quantification using multiple parameters (Wiemerslage and Lee, 2016). Besides, we may also find new plugins for mitochondrial morphology analysis on ImageJ software.

In addition, the U2OS cell model might not be the best for miniaturizing the mitochondrial morphology in neurodegenerative diseases. Because neurons behave differently from the actively dividing U2OS cells. And mitochondria play a more important role in neurons than other type of cells on the aspects of energy supply and transmission as well as membrane potential maintenance (Knott et al., 2008). Mitochondrial fragmentation may bring more significant and chronic effects on neurons under disease condition. Some neuroblastoma cells or neural cells differentiated from induced pluripotent stem cells (iPSC) would be more suitable cell models for studying mitochondrial dynamics in neurodegenerative diseases. Nevertheless, the U2OS cells model still provides important implications about mitochondrial fragmentation caused by AFG3L2 defects. The fragmentation phenotype not only results from OPA1 mediated fragmentation, but might also relate to respiratory defects. Counteracting these defects could also rescue the morphological changes of mitochondria, regardless of OPA1 degradation. This finding should be verified by more elaborate experiments with different cell types and quantitative methods, which would develop our understanding of the relationship between mitochondrial dynamics and mitochondrial respiration, giving rise to new ways of treating mitochondrial diseases.

Molecular basis of AOX has been widely studied in different plants both in vitro and in vivo, while its application in mammalian system is much more limited. The applications of AOX in engineered human cells and transgenic mice have implied a

way of rescuing the defective mitochondrial respiratory chain, mitigating the oxidative stress in the cell and curing mitochondrial diseases (Hakkaart et al., 2006; Dassa et al., 2009; El-Khoury et al., 2013). Based on these achievements, we tested the function and activity of AOX in the mouse brain and neuro-glia cells for the first time and generated a lentiviral vector for applying AOX in more mammalian cell types and tissues. The most exciting finding is that the AOX lentivirus significantly rescued the degree of mitochondrial fragmentation in the U2OS disease model cells established by *AFG3L2* gene silencing. Our study proposes an inspiring hint of applying AOX in future research or therapy of neurodegenerative diseases, especially those involve abnormal mitochondrial morphology. We also appeal that more functional studies about AOX should be done for the mammalian system. Because AOX is not only a promising candidate for developing efficient therapies but also a good tool for studying pathological mechanism of neurodegenerative diseases.

5. Conclusion

As the aim of this study has indicated, neurodegenerative diseases that are associated with mitochondrial dysfunction, have increasing impacts on human health and life currently. We propose a new way to treat these diseases with the alternative oxidase (AOX), which is proved in various studies to maintain the function of damaged mitochondrial respiratory chain and reduce the ROS production.

Since Ciona intestinalis AOX gene is absent in mammals, an engineered mouse model has been generated to express AOX all over the animal, with one copy of Ciona AOX gene inserted into the Rosa26 locus of C57Bl/6J mouse genome. Hemizygous AOXRosa26 transgenic mice were selected as the research materials. Our study first investigated the expression and function of AOX in the brain of this transgenic mouse model, finding that the amount and activity of AOX protein in the brain decreased along with age. In addition, we established a lentivirus vector to apply AOX gene to human cells, testing the therapeutic function of AOX in a neurodegenerative disease

model in vitro. And we observed that the fragmented mitochondrial phenotype of the AFG3L2 silencing disease model was alleviated by AOX despite of OPA1 cleavage, indicating that this mitochondrial phenotype is not only due to OPA1 cleavage, but also related to respiratory defects. This sheds a light on novel aspects that could help rescue mitochondrial morphological changes and implies the promising application of AOX in treating neurodegenerative diseases.

6. Acknowledgements

I would like to give great appreciation to my supervisor Kira Holmström. Thank you for your excellent and patient guide throughout this project. I still remember the day when I came to the lab for the first time, you taught me how to freeze the cells step by step. Gradually I have learnt to do all the experiments independently. Thank you for helping me revise the thesis again and again. Without you I could not have completed the delicate work. Thank you for your advices to all my presentations. The courage you gave let me become confident to talk in front of people. You are not only a good supervisor but also a good friend for me.

I would like also thank Prof. Howy Jacobs for allowing me to join this wonderful lab. Every group meeting and lab meeting you organized was a precious chance to learn and practice. You were always kind and generous to give everyone your honest suggestions, which I appreciated so much.

Great thanks to all the members in Howy's lab. Everyone was nice. I have learnt a lot from Luca, Praveen, Marten, Charley, Maarit and Sonja, who were very generous to share valuable experience and expertise with me. Udy and Troy were also very helpful whenever I needed.

Additionally, I would like to thank my roommates and my friends. Thank you for the company and happy time we spent together in Finland.

In the end, I would like to thank my mother for all her support and encouragement. You are the best mother in the world.

7. References

1. Aidt, F. H. *et al*. Dysfunctional mitochondrial respiration in the striatum of the Huntington's disease transgenic R6/2 mouse model. *PLoS Curr*. **5**, (2013).

2. Alberts, B. *et al*. Molecular Biology of the Cell, 6th edition. *Garland Science, New York.* 790-809 (2015).

3. Alexander, C. *et al*. OPA1, encoding a dynamin-related GTPase, is mutated in autosomal dominant optic atrophy linked to chromosome 3q28. *Nat. Genet.* **26**, 211 (2000).

4. Almajan, E. R. *et al*. AFG3L2 supports mitochondrial protein synthesis and Purkinje cell survival. *J. Clin. Invest.* **122**, 4048-4058 (2012).

5. Atorino, L. *et al*. Loss of m-AAA protease in mitochondria causes complex I deficiency and increased sensitivity to oxidative stress in hereditary spastic paraplegia. *J. Cell Biol.* **163**, 777-787 (2003).

6. Barber, R. D., Harmer, D. W., Coleman, R. A. & Clark, B. J. GAPDH as a housekeeping gene: analysis of GAPDH mRNA expression in a panel of 72 human tissues. *Physiol. Genomics* **21**, 389-395 (2005).

7. Berg, J. M., Tymoczko, J. L., Stryer, L. & Clarke, N. D. Biochemistry, 5th edition. Section 18.3, *W H freeman, New York,* (2002).

8. Berthold, D. A., Andersson, M. E. & Nordlund, P. New insight into the structure and function of the alternative oxidase. *Biochimica et Biophysica Acta (BBA)-Bioenergetics* **1460**, 241-254 (2000).

9. Berthold, D. A. & Stenmark, P. Membrane-bound diiron carboxylate proteins. *Annual review of plant biology* **54**, 497-517 (2003).

10. Bradford, M. M. A rapid and sensitive method for the quantitation of microgram quantities of protein utilizing the principle of protein-dye binding. *Anal. Biochem.* **72**, 248-254 (1976).

11. Brussino, A., Brusco, A. & Durr, A. in *GeneReviews(R)* (eds Pagon, R. A. et al.) (University of Washington, Seattle. GeneReviews is a registered trademark of the University of Washington, Seattle. All rights reserved, Seattle (WA), 2013).

12. CHAUDHURI, M., AJAYI, W., TEMPLE, S. & HILL, G. C. Identification and Partial Purification of a Stage-Specific 33 kDa Mitochondrial Protein as the Alternative Oxidase of the Trypanosoma brucei brucei Bloodstream Trypomastigotes. *J. Eukaryot. Microbiol.* **42**, 467-472 (1995).

13. Chen, H. & Chan, D. C. Mitochondrial dynamics–fusion, fission, movement, and mitophagy–in neurodegenerative diseases. *Hum. Mol. Genet.* **18**, R169-R176 (2009).

14. Chen, H. *et al*. Mitofusins Mfn1 and Mfn2 coordinately regulate mitochondrial fusion and are essential for embryonic development. *J. Cell Biol.* **160**, 189-200 (2003).

15. Chinnery, P. F. in *GeneReviews(R)* (eds Pagon, R. A. et al.) (University of Washington, Seattle. GeneReviews is a registered trademark of the University of Washington, Seattle. All rights reserved, Seattle (WA), 1993).

16. Cipolat, S. *et al*. Mitochondrial rhomboid PARL regulates cytochrome c release during apoptosis via OPA1-dependent cristae remodeling. *Cell* **126**, 163-175 (2006).

17. Clifton, R., Millar, A. H. & Whelan, J. Alternative oxidases in Arabidopsis: a comparative analysis of differential expression in the gene family provides new insights into function of non-phosphorylating bypasses. *Biochimica et Biophysica Acta (BBA)-Bioenergetics* **1757**, 730-741 (2006).

18. Cooper, G. M. & Hausman, R. E. The Cell. *Sinauer Associates Sunderland*, (2000).

19. Dassa, E. P. *et al*. Expression of the alternative oxidase complements cytochrome c oxidase deficiency in human cells. *EMBO Mol. Med.* **1**, 30-36 (2009).

20. De Clercq, I. *et al*. The membrane-bound NAC transcription factor ANAC013 functions in mitochondrial retrograde regulation of the oxidative stress response in Arabidopsis. *Plant Cell* **25**, 3472-3490 (2013).

21. Delettre, C. *et al*. Mutation spectrum and splicing variants in the OPA1 gene. *Hum. Genet.* **109**, 584-591 (2001).

22. Delettre, C. *et al*. Nuclear gene OPA1, encoding a mitochondrial dynamin-related protein, is mutated in dominant optic atrophy. *Nat. Genet.* **26**, 207 (2000).

23. Detmer, S. A. & Chan, D. C. Functions and dysfunctions of mitochondrial dynamics. *Nature reviews.Molecular cell biology* **8**, 870 (2007).

24. Di Bella, D. *et al*. Mutations in the mitochondrial protease gene AFG3L2 cause dominant hereditary ataxia SCA28. *Nat. Genet.* **42**, 313-321 (2010).

25. DiMauro, S. & Schon, E. A. Mitochondrial respiratory-chain diseases. *N. Engl. J. Med.* **348**, 2656-2668 (2003).

26. Djafarzadeh, S. & Jakob, S. M. High-resolution Respirometry to Assess Mitochondrial Function in Permeabilized and Intact Cells. *JoVE (Journal of Visualized Experiments)*, e54985-e54985 (2017).

27. Dull, T. *et al*. A third-generation lentivirus vector with a conditional packaging system. *J. Virol.* **72**, 8463-8471 (1998).

28. Duvezin-Caubet, S. *et al*. Proteolytic processing of OPA1 links mitochondrial dysfunction to alterations in mitochondrial morphology. *J. Biol. Chem.* **281**, 37972-37979 (2006).

29. Ehses, S. *et al*. Regulation of OPA1 processing and mitochondrial fusion by m-AAA protease isoenzymes and OMA1. *J. Cell Biol.* **187**, 1023-1036 (2009).

30. El-Khoury, R. *et al*. Alternative oxidase expression in the mouse enables bypassing cytochrome c oxidase blockade and limits mitochondrial ROS overproduction. *PLoS Genet* **9**, e1003182 (2013).

31. El-Khoury, R. *et al*. Expression of the alternative oxidase mitigates beta-amyloid production and toxicity in model systems. *Free Radical Biology and Medicine* **96**, 57-66 (2016).

32. El-Khoury, R. *et al*. Engineering the alternative oxidase gene to better understand and counteract mitochondrial defects: state of the art and perspectives. *Br. J. Pharmacol.* **171**, 2243-2249 (2014).

33. Federico, A. *et al*. Mitochondria, oxidative stress and neurodegeneration. *J. Neurol. Sci.* **322**, 254-262 (2012).

34. Ferguson, R. E. *et al*. Housekeeping proteins: a preliminary study illustrating some limitations as useful references in protein expression studies. *Proteomics* **5**, 566-571 (2005).

35. Fernandez-Ayala, D. J. *et al*. Expression of the Ciona intestinalis alternative oxidase (AOX) in Drosophila complements defects in mitochondrial oxidative phosphorylation. *Cell metabolism* **9**, 449-460 (2009).

36. Filler, K. *et al*. Association of mitochondrial dysfunction and fatigue: a review of the literature. *BBA clinical* **1**, 12-23 (2014).

37. Frezza, C. *et al*. OPA1 controls apoptotic cristae remodeling independently from mitochondrial fusion. *Cell* **126**, 177-189 (2006).

38. Friedrich, G. & Soriano, P. Promoter traps in embryonic stem cells: a genetic screen to identify and mutate developmental genes in mice. *Genes Dev.* **5**, 1513-1523 (1991).

39. Giraud, E., Van Aken, O., Ho, L. H. & Whelan, J. The transcription factor ABI4 is a regulator of mitochondrial retrograde expression of ALTERNATIVE OXIDASE1a. *Plant Physiol.* **150**, 1286-1296 (2009).

40. Grant, N. *et al*. Two cys or not two cys? That is the question; alternative oxidase in the thermogenic plant sacred Lotus. *Plant Physiol.* **150**, 987-995 (2009).

41. Green, D. R. & Reed, J. C. Mitochondria and apoptosis. *Science* **281**, 1309 (1998).

42. Griparic, L., Kanazawa, T. & van der Bliek, A. M. Regulation of the mitochondrial dynamin-like protein Opa1 by proteolytic cleavage. *J. Cell Biol.* **178**, 757-764 (2007).

43. Guerrero-Castillo, S., Cabrera-Orefice, A., Vázquez-Acevedo, M., González-Halphen, D. & Uribe-Carvajal, S. During the stationary growth phase, Yarrowia lipolytica prevents the overproduction of reactive oxygen species by activating an uncoupled mitochondrial respiratory pathway. *Biochimica et Biophysica Acta (BBA)-Bioenergetics* **1817**, 353-362 (2012).

44. Hakkaart, G. A., Dassa, E. P., Jacobs, H. T. & Rustin, P. Allotopic expression of a mitochondrial alternative oxidase confers cyanide resistance to human cell respiration. *EMBO Rep.* **7**, 341-345 (2006).

45. Henze, K. & Martin, W. Evolutionary biology: essence of mitochondria. *Nature* **426**, 127-128 (2003).

46. Hitoshi, N., Ken-ichi, Y. & Jun-ichi, M. Efficient selection for high-expression transfectants with a novel eukaryotic vector. *Gene* **108**, 193-199 (1991).

47. Irion, S. *et al*. Identification and targeting of the ROSA26 locus in human embryonic stem cells. *Nat. Biotechnol.* **25**, 1477 (2007).

48. Ishihara, N., Fujita, Y., Oka, T. & Mihara, K. Regulation of mitochondrial morphology through proteolytic cleavage of OPA1. *EMBO J.* **25**, 2966-2977 (2006).

49. Juhola, M. K., Shah, Z. H., Grivell, L. A. & Jacobs, H. T. The mitochondrial inner membrane AAA metalloprotease family in metazoans. *FEBS Lett.* **481**, 91-95 (2000).

50. Karbowski, M. & Neutzner, A. Neurodegeneration as a consequence of failed mitochondrial maintenance. *Acta Neuropathol.* **123**, 157-171 (2012).

51. Kemppainen, K. K. *et al*. Expression of alternative oxidase in Drosophila ameliorates diverse phenotypes due to cytochrome oxidase deficiency. *Hum. Mol. Genet.* **23**, 2078-2093 (2014).

52. Khan, N. A., Govindaraj, P., Meena, A. K. & Thangaraj, K. Mitochondrial disorders: challenges in diagnosis & treatment. *Indian J. Med. Res.* **141**, 13-26 (2015).

53. Kim, H. *et al*. Structure of antimycin A1, a specific electron transfer inhibitor of ubiquinol− cytochrome c oxidoreductase. *J. Am. Chem. Soc.* **121**, 4902-4903 (1999).

54. Kim, M. J. *et al*. Mitochondrial complexes I and II are more susceptible to autophagy deficiency in mouse β-cells. *Endocrinology and Metabolism* **30**, 65-70 (2015).

55. Kirichok, Y., Krapivinsky, G. & Clapham, D. E. The mitochondrial calcium uniporter is a highly selective ion channel. *Nature* **427**, 360-364 (2004).

56. Knott, A. B. & Bossy-Wetzel, E. Impairing the mitochondrial fission and fusion balance: a new mechanism of neurodegeneration. *Ann. N. Y. Acad. Sci.* **1147**, 283-292 (2008).

57. Knott, A. B., Perkins, G., Schwarzenbacher, R. & Bossy-Wetzel, E. Mitochondrial fragmentation in neurodegeneration. *Nature Reviews Neuroscience* **9**, 505-518 (2008).

58. Kondadi, A. K. AFG3L2 deficiency impairs axonal transport of mitochondria dependent on ROS and tau levels. *Universität zu Köln*, (2014).

59. Kondadi, A. K. *et al*. Loss of the m-AAA protease subunit AFG3L2 causes mitochondrial transport defects and tau hyperphosphorylation. *EMBO J.* **33**, 1011-1026 (2014).

60. Krebs, H. A. & Johnson, W. A. Acetopyruvic acid (alphagamma-diketovaleric acid) as an intermediate metabolite in animal tissues. *Biochem. J.* **31**, 772-779 (1937).

61. Krebs, H. A. & Johnson, W. A. Metabolism of ketonic acids in animal tissues. *Biochem. J.* **31**, 645-660 (1937).

62. Lee, Y. J., Jeong, S. Y., Karbowski, M., Smith, C. L. & Youle, R. J. Roles of the mammalian mitochondrial fission and fusion mediators Fis1, Drp1, and Opa1 in apoptosis. *Mol. Biol. Cell* **15**, 5001-5011 (2004).

63. Lenaers, G. *et al*. OPA1 functions in mitochondria and dysfunctions in optic nerve. *Int. J. Biochem. Cell Biol.* **41**, 1866-1874 (2009).

64. Leonard, A. P. *et al*. Quantitative analysis of mitochondrial morphology and membrane potential in living cells using high-content imaging, machine learning, and morphological binning. *Biochimica et Biophysica Acta (BBA)-Molecular Cell Research* **1853**, 348-360 (2015).

65. Leonard, J. & Schapira, A. H. Mitochondrial respiratory chain disorders I: mitochondrial DNA defects. *The Lancet* **355**, 299-304 (2000).

66. Leonard, J. & Schapira, A. H. Mitochondrial respiratory chain disorders II: neurodegenerative disorders and nuclear gene defects. *The Lancet* **355**, 389-394 (2000).

67. Li, Z. & Xing, D. Mechanistic study of mitochondria-dependent programmed cell death induced by aluminium phytotoxicity using fluorescence techniques. *J. Exp. Bot.* **62**, 331-343 (2010).

68. Lin, M. T. & Beal, M. F. Mitochondrial dysfunction and oxidative stress in neurodegenerative diseases. *Nature* **443**, 787-795 (2006).

69. Liu, W. *et al*. Mutations in cytochrome c oxidase subunit VIa cause neurodegeneration and motor dysfunction in Drosophila. *Genetics* **176**, 937-946 (2007).

70. Mali, P. *et al*. Improved efficiency and pace of generating induced pluripotent stem cells from human adult and fetal fibroblasts. *Stem Cells* **26**, 1998-2005 (2008).

71. Maltecca, F. *et al*. Respiratory dysfunction by AFG3L2 deficiency causes decreased mitochondrial calcium uptake via organellar network fragmentation. *Hum. Mol. Genet.* **21**, 3858-3870 (2012).

72. Maltecca, F. *et al*. The mitochondrial protease AFG3L2 is essential for axonal development. *J. Neurosci.* **28**, 2827-2836 (2008).

73. Maltecca, F. *et al*. Purkinje neuron Ca2+ influx reduction rescues ataxia in SCA28 model. *J. Clin. Invest.* **125**, 263-274 (2015).

74. Maltecca, F. *et al*. Haploinsufficiency of AFG3L2, the gene responsible for spinocerebellar ataxia type 28, causes mitochondria-mediated Purkinje cell dark degeneration. *J. Neurosci.* **29**, 9244-9254 (2009).

75. Manczak, M. & Reddy, P. H. Abnormal interaction between the mitochondrial fission protein Drp1 and hyperphosphorylated tau in Alzheimer's disease neurons: implications for mitochondrial dysfunction and neuronal damage. *Hum. Mol. Genet.* **21**, 2538-2547 (2012).

76. Martin, W. & Mentel, M. The origin of mitochondria. *Nature Education* **3**, 58 (2010).

77. Matsukawa, K., Kamata, T. & Ito, K. Functional expression of plant alternative oxidase decreases antimycin A-induced reactive oxygen species production in human cells. *FEBS Lett.* **583**, 148-152 (2009).

78. Matus-Ortega, M. *et al*. New complexes containing the internal alternative NADH dehydrogenase (Ndi1) in mitochondria of Saccharomyces cerevisiae. *Yeast* **32**, 629-641 (2015).

79. Maxwell, D. P., Wang, Y. & McIntosh, L. The alternative oxidase lowers mitochondrial reactive oxygen production in plant cells. *Proc. Natl. Acad. Sci. U. S. A.* **96**, 8271-8276 (1999).

80. McBride, H. M., Neuspiel, M. & Wasiak, S. Mitochondria: more than just a powerhouse. *Current biology* **16**, R551-R560 (2006).

81. McDonald, A. E. & Vanlerberghe, G. C. Branched mitochondrial electron transport in the Animalia: presence of alternative oxidase in several animal phyla. *IUBMB Life* **56**, 333-341 (2004).

82. McDonald, A. E., Vanlerberghe, G. C. & Staples, J. F. Alternative oxidase in animals: unique characteristics and taxonomic distribution. *J. Exp. Biol.* **212**, 2627-2634 (2009).

83. McIntosh, L. Molecular biology of the alternative oxidase. *Plant Physiol.* **105**, 781-786 (1994).

84. Meeuse, B. J. Thermogenic respiration in aroids. *Annual Review of Plant Physiology* **26**, 117-126 (1975).

85. Mitchell, P. Chemiosmotic coupling in oxidative and photosynthetic phosphorylation. *Biological Reviews* **41**, 445-501 (1966).

86. Mizuguchi, H., Xu, Z., Ishii-Watabe, A., Uchida, E. & Hayakawa, T. IRES-dependent second gene expression is significantly lower than cap-dependent first gene expression in a bicistronic vector. *Molecular Therapy* **1**, 376-382 (2000).

87. Mozo, J., Emre, Y., Bouillaud, F., Ricquier, D. & Criscuolo, F. Thermoregulation: what role for UCPs in mammals and birds? *Biosci. Rep.* **25**, 227-249 (2005).

88. Murphy, A. D., Doeller, J. E., Hearn, B. & Lang-Unnasch, N. Plasmodium falciparum: cyanide-resistant oxygen consumption. *Exp. Parasitol.* **87**, 112-120 (1997).

89. Naldini, L. *et al*. In vivo gene delivery and stable transduction of nondividing cells by a lentiviral vector. *Science-AAAS-Weekly Paper Edition* **272**, 263-267 (1996).

90. Naldini, L., Blomer, U., Gage, F. H., Trono, D. & Verma, I. M. Efficient transfer, integration, and sustained long-term expression of the transgene in adult rat brains injected with a lentiviral vector. *Proc. Natl. Acad. Sci. U. S. A.* **93**, 11382-11388 (1996).

91. Nargang, F. E. *et al*. Identification of genes required for alternative oxidase production in the Neurospora crassa gene knockout library. *G3 (Bethesda)* **2**, 1345-1356 (2012).

92. Olichon, A. *et al*. Loss of OPA1 perturbates the mitochondrial inner membrane structure and integrity, leading to cytochrome c release and apoptosis. *J. Biol. Chem.* **278**, 7743-7746 (2003).

93. Otera, H. & Mihara, K. Molecular mechanisms and physiologic functions of mitochondrial dynamics. *The Journal of Biochemistry* **149**, 241-251 (2011).

94. Pagon, R. A. *et al*. Mitochondrial Disorders Overview. *GeneReviews® [Internet]. Seattle (WA): University of Washington, Seattle,* 1993-2018 (2010).

95. Patel, M. & Barsotti, R. Measuring recovery in mitochondrial respiration after varying lengths of reperfusion time. *Philadelphia College of Osteopathic Medicine* (2015).

96. Paulson, H. L. The spinocerebellar ataxias. *J. Neuroophthalmol.* **29**, 227-237 (2009).

97. Pelletier, J. & Sonenberg, N. Internal initiation of translation of eukaryotic mRNA directed by a sequence derived from poliovirus RNA. *Nature* **334**, 320-325 (1988).

98. Peng, L., Parpura, V. & Verkhratsky, A. EDITORIAL Neuroglia as a Central Element of Neurological Diseases: An Underappreciated Target for Therapeutic Intervention. *Current Neuropharmacology* **12**, 303-307 (2014).

99. Pesta, D. & Gnaiger, E. High-resolution respirometry: OXPHOS protocols for human cells and permeabilized fibers from small biopsies of human muscle. *Mitochondrial bioenergetics: methods and protocols*, 25-58 (2012).

100. Pierson, T. M. *et al*. Whole-exome sequencing identifies homozygous AFG3L2 mutations in a spastic ataxia-neuropathy syndrome linked to mitochondrial m-AAA proteases. *PLoS genetics* **7**, e1002325 (2011).

101. Rogov, A., Sukhanova, E., Uralskaya, L., Aliverdieva, D. & Zvyagilskaya, R. Alternative oxidase: distribution, induction, properties, structure, regulation, and functions. *Biochemistry (Moscow)* **79**, 1615-1634 (2014).

102. Schaefer, A. M. *et al*. Prevalence of mitochondrial DNA disease in adults. *Ann. Neurol.* **63**, 35-39 (2008).

103. Schapira, A. H. Mitochondrial diseases. *The Lancet* **379**, 1825-1834 (2012).

104. Sierra-Campos, E., Velazquez, I., Matuz-Mares, D., Villavicencio-Queijeiro, A. & Pardo, J. Functional properties of the Ustilago maydis alternative oxidase under oxidative stress conditions. *Mitochondrion* **9**, 96-102 (2009).

105. Skatchkov, S., Woodbury, M. & Eaton, M. The Role of Glia in Stress: Polyamines and BrainDisorders. *Psychiatric Clinics of North America* **37**, 653-78 (2014).

106. Song, Z., Chen, H., Fiket, M., Alexander, C. & Chan, D. C. OPA1 processing controls mitochondrial fusion and is regulated by mRNA splicing, membrane potential, and Yme1L. *J. Cell Biol.* **178**, 749-755 (2007).

107. Srinivas, S. *et al*. Cre reporter strains produced by targeted insertion of EYFP and ECFP into the ROSA26 locus. *BMC developmental biology* **1**, 4 (2001).

108. Stachel, S. E. & Nester, E. W. The genetic and transcriptional organization of the vir region of the A6 Ti plasmid of Agrobacterium tumefaciens. *EMBO J.* **5**, 1445-1454 (1986).

109. Stegmeier, F., Hu, G., Rickles, R. J., Hannon, G. J. & Elledge, S. J. A lentiviral microRNA-based system for single-copy polymerase II-regulated RNA interference in mammalian cells. *Proc. Natl. Acad. Sci. U. S. A.* **102**, 13212-13217 (2005).

110. Su, B. *et al*. Abnormal mitochondrial dynamics and neurodegenerative diseases. *Biochimica et Biophysica Acta (BBA)-Molecular Basis of Disease* **1802**, 135-142 (2010).

111. Suomalainen, A. *Therapy for mitochondrial disorders: little proof, high research activity, some promise* (Seminars in Fetal and Neonatal Medicine Ser. 16, Elsevier, 2011).

112. Szibor, M. *et al*. Broad AOX expression in a genetically tractable mouse model does not disturb normal physiology. *Dis. Model. Mech.* **10**, 163-171 (2017).

113. Tatsuta, T. & Langer, T. Quality control of mitochondria: protection against neurodegeneration and ageing. *EMBO J.* **27**, 306-314 (2008).

114. Tyynismaa, H. & Suomalainen, A. Mouse models of mitochondrial DNA defects and their relevance for human disease. *EMBO Rep.* **10**, 137-143 (2009).

115. Uribe, D. & Khachatourians, G. G. Identification and characterization of an alternative oxidase in the entomopathogenic fungus Metarhizium anisopliae. *Can. J. Microbiol.* **54**, 119-127 (2008).

116. Van Aken, O., Zhang, B., Law, S., Narsai, R. & Whelan, J. AtWRKY40 and AtWRKY63 modulate the expression of stress-responsive nuclear genes encoding mitochondrial and chloroplast proteins. *Plant Physiol.* **162**, 254-271 (2013).

117. Vanlerberghe, G. C. Alternative oxidase: a mitochondrial respiratory pathway to maintain metabolic and signaling homeostasis during abiotic and biotic stress in plants. *International Journal of Molecular Sciences* **14**, 6805-6847 (2013).

118. Vanlerberghe, G. C. & McIntosh, L. Mitochondrial electron transport regulation of nuclear gene expression. Studies with the alternative oxidase gene of tobacco. *Plant Physiol.* **105**, 867-874 (1994).

119. Vanlerberghe, G. C. & McLntosh, L. Signals Regulating the Expression of the Nuclear Gene Encoding Alternative Oxidase of Plant Mitochondria. *Plant Physiol.* **111**, 589-595 (1996).

120. Veiga, A., Arrabaça, J. D. & Loureiro-Dias, M. C. Cyanide-resistant respiration is frequent, but confined to yeasts incapable of aerobic fermentation. *FEMS Microbiol. Lett.* **190**, 93-97 (2000).

121. Voet, D., Voet, J. G. & Pratt, C. W. in *Fundamentals of biochemistry* (Wiley, 2013).

122. Vowinckel, J., Hartl, J., Butler, R. & Ralser, M. MitoLoc: A method for the simultaneous quantification of mitochondrial network morphology and membrane potential in single cells. *Mitochondrion* **24**, 77-86 (2015).

123. Walker, R., Saha, L., Hill, G. C. & Chaudhuri, M. The effect of over-expression of the alternative oxidase in the procyclic forms of Trypanosoma brucei. *Mol. Biochem. Parasitol.* **139**, 153-162 (2005).

124. Westermann, B. Bioenergetic role of mitochondrial fusion and fission. *Biochimica et Biophysica Acta (BBA)-Bioenergetics* **1817**, 1833-1838 (2012).

125. Wiemerslage, L. & Lee, D. Quantification of mitochondrial morphology in neurites of dopaminergic neurons using multiple parameters. *J. Neurosci. Methods* **262**, 56-65 (2016).

126. Yu-Wai-Man, P. *et al*. Multi-system neurological disease is common in patients with OPA1 mutations. *Brain* **133**, 771-786 (2010).

127. Züchner, S. *et al*. Mutations in the mitochondrial GTPase mitofusin 2 cause Charcot-Marie-Tooth neuropathy type 2A. *Nat. Genet.* **36**, 449-451 (2004).